Atmos. Chem. Phys., 25, 12811-12830, 2025 https://doi.org/10.5194/acp-25-12811-2025 © Author(s) 2025. This work is distributed under the Creative Commons Attribution 4.0 License.





Divergent changes in aerosol optical hygroscopicity and new particle formation during a heatwave of summer 2022

Yuhang Hao^{1,★}, Peizhao Li^{1,★}, Yafeng Gou¹, Zhenshuai Wang¹, Mi Tian¹, Yang Chen², Ye Kuang³, Hanbing Xu⁴, Fenglian Wan¹, Yuqian Luo¹, Wei Huang⁵, and Jing Chen^{1,6}

¹College of Environment and Ecology, Chongqing University, Chongqing 400045, China ²Center for the Atmospheric Environment Research, Chongqing Institute of Green and Intelligent Technology, Chinese Academy of Sciences, Chongqing 400714, China

³Institute for Environmental and Climate Research, Jinan University, Guangzhou 511443, China ⁴Experimental Teaching Center, Sun Yat-sen University, Guangzhou 510275, China ⁵National Meteorological Center, China Meteorological Administration, Beijing 100081, China

⁶Key Laboratory of Three Gorges Reservoir Region's Eco-Environment, Ministry of Education,

Chongqing University, Chongqing 400045, China

These authors contributed equally to this work.

Correspondence: Jing Chen (chen.jing@cqu.edu.cn)

Received: 17 October 2024 - Discussion started: 15 November 2024 Revised: 4 August 2025 – Accepted: 8 August 2025 – Published: 15 October 2025

Abstract. As a crucial climate-forcing driver, the aerosol optical enhancement factor (f(RH)) is significantly modulated by chemical compositions and the evolution of particle number size distribution (PNSD), e.g., during new particle formation (NPF). However, mechanisms regulating aerosol optical hygroscopicity during different NPF days, particularly those under heatwaves due to global warming, remain poorly understood. In the hot summer of 2022 in urban Chongqing of southwest China, simultaneous measurements of aerosol optical and hygroscopic properties, PNSD, and bulk chemical compositions were conducted. Two distinct types of NPFs were identified: NPFs with relatively polluted periods (NPF_{polluted}) and clean cases during heatwave-dominated periods (NPF_{clean, HW}). Compared to the NPF_{polluted} events, NPF_{clean, HW} occurred approximately 1 h earlier, and the subsequent growth was prolonged, accompanied by a smaller aerosol effective radius (R_{eff}) and lower formation/growth rate during heatwaves. This agreed with the concurrently increased aerosol hemispheric backscattering fraction and scattering Ångström exponent. A generally higher f(RH) was observed on NPF days than in non-event cases, partly attributable to distinct changes in PNSD patterns during NPF days. Moreover, heatwaveinduced stronger photooxidation may intensify the formation of more hygroscopic secondary components and prolong the atmospheric aging/subsequent growth of both pre-existing and newly formed particles, largely contributing to the enhanced f(RH), especially during NPF_{clean, HW} days. The higher f(RH) and lowered R_{eff} could synergistically elevate the aerosol direct radiative forcing, specifically under persistent heatwave conditions. Further in-depth exploration of molecular-level characterizations and the aerosol radiative impacts of both direct and indirect interactions under heatwaves in a warming climate is recommended.

1 Introduction

Weather extremes (e.g., heatwaves) have become more and more frequent and intense, largely due to global climate change, and heatwave-driven environmental, climatic, and health effects have garnered widespread attention (Hauser et al., 2016; Sun et al., 2016). The China Climate Bulletin 2022 confirmed that the national average temperature had reached an unprecedented high level since 2012 (China Meteorological Administration, 2022), and the risk of heatwaves in China will persist and potentially intensify in the future (Guo et al., 2016; Li et al., 2017). Extreme-heatwave events could pose significant threats to human health, the survival of organisms, agriculture, and socio-economic activities (e.g., power supply restrictions) (Brooke Anderson and Bell, 2011; Ma et al., 2021; Su, 2021). Moreover, heatwaves can trigger natural disasters such as droughts and wildfires, affecting social stability (Sharma and Mujumdar, 2017).

Heatwaves can also affect atmospheric physical and chemical processes by modulating ambient meteorological conditions. Specifically, extremely high temperature weather is typically characterized by a combination of intensified solar radiation with elevated temperature and low humidity levels. This could significantly affect the formation and evolution of secondary aerosols in the atmosphere (Bousiotis et al., 2021; Hamed et al., 2011; Kurtén et al., 2007), given that air temperature is crucial for chemical reactions (Xu et al., 2011). New particle formation (NPF) serves as a crucial source of atmospheric particulate matter and plays a significant role in the secondary transformation processes in the atmosphere (Zhu et al., 2021). Generally, NPF involves the initial formation of thermodynamically stable clusters from condensable vapors (e.g., ammonia, sulfuric acid, and organic precursor gases) and subsequent growth of the formed clusters, eventually reaching detectable sizes or even larger dimensions (Kerminen et al., 2018; Kulmala, 2003; Kulmala et al., 2012). Over time, these newly formed particles have the potential to serve as cloud condensation nuclei (CCN), thereby impacting the global climate (Salma et al., 2016). NPF events normally introduce a sharp increase in the number concentration of nucleation mode particles within a short time, altering the particle number size distribution (PNSD). These variations in PNSD likely influence the intrinsic physicochemical properties of aerosols, such as the optical hygroscopicity (Chen et al., 2014; Titos et al., 2016; Zhao et al., 2019).

Aerosol hygroscopicity plays a critical role in the atmospheric environment and climate change, given the complex interaction between aerosol particles and water vapor (Zhao et al., 2019; Zieger et al., 2011). Water uptake by aerosols not only alters the particle size and composition (e.g., as reflected in the aerosol refractive index) but also impacts aerosol scattering efficiency, which further contributes to the uncertainty in aerosol radiative forcing estimation (Titos et al., 2016, 2021). The aerosol optical hygroscopicity parameter, f(RH), defined as the ratio of the scattering coefficient at a certain

RH to that of the dry condition, has been widely used to describe the aerosol scattering enhancement through water uptake (Covert et al., 1972; Titos et al., 2016; Zhao et al., 2019). Numerous studies have demonstrated that f(RH) is influenced by size distribution, in addition to particle chemical composition (Chen et al., 2014; Kuang et al., 2017; Petters and Kreidenweis, 2007; Quinn et al., 2005). There is currently limited research on the variations in aerosol optical hygroscopicity during NPF days despite significant changes in aerosol size distributions and chemical compositions, partly due to the fact that newly formed particles insignificantly affect the optical properties of aerosols (Kuang et al., 2018). However, previous studies have observed an enhancement in aerosol hygroscopicity (Cheung et al., 2020; Wu et al., 2015, 2016) and extinction coefficients (Shen et al., 2011; Sun et al., 2024) during the subsequent growth of NPF. It is suggested that the influence of NPF on aerosol hygroscopicity was likely due to changes in aerosol chemical composition at different stages of NPF events (Cheung et al., 2020), whereas the subsequent particle growth associated with NPF events can significantly affect particle hygroscopicity as well (Wu et al., 2016). Although previous studies have shown the dependences of aerosol hygroscopicity on chemical composition (Petters and Kreidenweis, 2007; Titos et al., 2016; Zhao et al., 2019) (e.g., variations in the composition of precursor species during NPF events), it is important to acknowledge that the utilized chemical compositions of NPF were either from PM_{2.5} or from PM₁ bulk data. This may differ from the corresponding composition of newly formed ultrafine particles, primarily in the nucleation and Aitken modes, further introducing bias in exploring the impacts of NPF and subsequent growth on aerosol optical hygroscopicity. Hence, more comprehensive investigations on the mechanisms influencing aerosol optical hygroscopicity from different perspectives are required, e.g., for the aspects of the evolution of particle size distribution in modulating aerosol optical and hygroscopic properties (Tang et al., 2019; Zhao et al., 2019). Additionally, field observations on f(RH) under extreme-weather conditions (e.g., heatwaves) are rather scarce, largely hindering our understanding of how weather extremes (e.g., extremely high temperature) influence the optical hygroscopic properties of aerosols. This knowledge gap further impedes a comprehensive understanding of the aerosol water uptake property and resulting effects on air quality and the climate under varied synoptic conditions.

During the summer of 2022, a rare heatwave event raged throughout China, especially in the Sichuan–Chongqing region of southwest China (Chen et al., 2024; Wang et al., 2024), with the daily maximum temperature exceeding 40° and lasting for 29 d, as observed at the Beibei meteorological station in Chongqing (Hao et al., 2023). This persistent heatwave not only impacted residents' daily lives significantly, but also affected aerosol optical and hygroscopic properties, likely through changed aerosol physicochemical characteristics and relevant atmospheric processing during this period.

In this study, a field observation was conducted by using a combination of a home-built humidified nephelometer system and a scanning mobility particle sizer (SMPS), along with total suspended particle (TSP) filter sampling. A main goal of this study is to investigate the influence of heatwaves on both aerosol optical hygroscopicity and the NPF with subsequent growth events, along with the related discrepancies. Furthermore, we aimed to explore the mechanisms behind the variability in f(RH) under different meteorological conditions and diverse NPF events. This study will further enrich insights into the potential environmental impacts due to variations in aerosol optical hygroscopicity and size distribution, specifically under heatwaves in a changing climate.

2 Data and methods

2.1 Field observation

A continuous field observation on aerosol optical, hygroscopic, and chemical properties was carried out from 29 July to 19 August 2022. A detailed description of the observation site is available in Supplement S1. During the observation period, urban Chongqing suffered a rare heatwave (Fig. S1; Chen et al., 2024; Wang et al., 2024), which significantly affected local transportation and industrial activities (Hao et al., 2023). The China Meteorological Administration (CMA) defines heatwaves as 3 or more consecutive days with daily maximum temperature (T_{max}) above 35 °C (http://www.cmastd.cn/standardView.jspx?id=2103 (last access: 7 October 2025); Guo et al., 2016; Sun et al., 2014; Tan et al., 2007). Since there is no unified definition of heatwaves worldwide, the whole study period was categorized into two stages according to CMA's criteria for daily T_{max} records and the excess heat factor (EHF) metric proposed by Nairn and Fawcett (2014) (Fig. S2a): (1) the normally hot period from 29 July to 6 August (marked as P1) and (2) the heatwavedominated period from 7-19 August (marked as P2), characterized by the consistent occurrence of T_{max} exceeding 38 °C (approximately the lowest 25th percentile of temperature records for the whole observation period; Fig. S2b).

2.2 Instrumentation and methods

2.2.1 Measurements of aerosol optical hygroscopicity

The humidified nephelometer system, consisting of two three-wavelength (i.e., 450, 525, and 635 nm) nephelometers (Aurora 3000, Ecotech Inc.) and a humidification unit, was used to determine the aerosol light scattering enhancement factor, f(RH). Ambient air was first dried through a Nafion dryer (MD-700, Perma Pure LLC) to ensure RH <35 %, then split into two streams for both dry and humidified nephelometers operated in parallel. The flow rate for each nephelometer was 2.6 LPM. The aerosol scattering ($\sigma_{sca, \lambda}$) and backscattering coefficients ($\sigma_{bsca, \lambda}$) were detected in a dry state (RH < 35 %) and at a controlled RH level of 85 \pm 1 %,

respectively, with the humidification efficiency regulated automatically by a temperature-controlled water bath. More details on the home-built humidified nephelometer system are available in Kuang et al. (2017, 2020) and Xue et al. (2022).

Hence, f(RH) could be calculated as the ratio of the aerosol scattering coefficient at a predefined RH ($\sigma_{sca, RH}$) to the dry ($\sigma_{sca, dry}$) state; i.e., $f(RH) = \sigma_{sca, RH}/\sigma_{sca, dry}$ (Covert et al., 1972). In this study, the f(RH) discussed is mainly targeted at the 525 nm wavelength, unless otherwise specified. More information about the measurements of the humidified nephelometer system is illustrated in Sect. S2 of the Supplement.

In addition to f(RH), aerosol optical parameters, such as the scattering Ångström exponent (SAE; Schuster et al., 2006) and hemispheric backscattering fraction (HBF; Collaud Coen et al., 2007), were calculated as below:

$$SAE_{\lambda 1/\lambda 2} = \frac{-\ln\left(\sigma_{sca,\lambda 1}/\sigma_{sca,\lambda 2}\right)}{\ln\left(\lambda 1/\lambda 2\right)},\tag{1}$$

$$HBF_{\lambda} = \frac{\sigma_{bsca,\lambda}}{\sigma_{sca,\lambda}},\tag{2}$$

where $\sigma_{sca, \lambda}$ and $\sigma_{bsca, \lambda}$ represent the aerosol scattering and backscattering coefficients at a specific wavelength λ (e.g., $\lambda 1, \lambda 2$), respectively.

Both HBF and SAE reflect crucial optical properties of aerosols, e.g., an elevated HBF (or SAE) generally signifies a higher concentration (or a smaller particle size) of fine particles within the aerosol population (Jefferson et al., 2017; Kuang et al., 2017; Luoma et al., 2019). The HBF and SAE discussed in this study are targeted at the dry condition, unless otherwise specified. Based on the measurements with the humidified nephelometer system, the equivalent aerosol liquid water content (ALWC) and the corresponding fraction of ALWC (f_W) can also be obtained (Kuang et al, 2018; see Sect. S2 of the Supplement).

The SMPS-measured concurrent particle number size distributions were further utilized to calculate the aerosol effective radius ($R_{\rm eff}$) and parameters representative of NPF events, e.g., the formation rate (FR) and growth rate (GR) of new particles, condensation sink (CS), and coagulation sink (CoagS) (Dal Maso et al., 2005; Kulmala et al., 2012). More details are provided in the Supplement (Sect. S5).

Results of the offline chemical analysis with TSP filter samples are provided in Sect. S3 and Fig. S3. It should be noted that certain secondary organics and crustal elements (e.g., Ca²⁺, Mg²⁺) that could exhibit a broader size distribution may contribute to the observed discrepancy in the total mass concentration between the 24 h TSP samples and daily mean PM_{2.5} (of similar temporal variations; Fig. S3) (Duan et al., 2024; Kim et al., 2020; Xu et al., 2021). Nonetheless, previous studies have reported that key components such as SNA (i.e., SO₄²⁻, NO₃⁻, and NH₄⁺) and primary organics of PM_{2.5} (or PM₁₀) were predominantly concentrated within the submicron size range (An et al., 2024; Bae et al., 2019;

Chen et al., 2019; Duan et al., 2024; Kim et al., 2020; Xu et al., 2024). While the use of TSP samples contains some uncertainties, the bulk chemical information remains reasonable for characterizing the optical and hygroscopic properties of PM_{2.5}. Descriptions of simultaneously collected meteorological and air quality data can be found in Sect. S4, and the 48 h/72 h backward trajectory analysis is given in Sect. S5 of the Supplement.

2.2.2 Determination of the aerosol direct radiative forcing (ADRF) enhancement factor

Given the high sensitivity of aerosol optical properties (e.g., f(RH)) to the changes in RH under real atmospheric conditions, the influence of RH, or rather the aerosol hygroscopicity, on ADRF can be quantitatively estimated with the radiative transfer model using the following equation (Chylek and Wong, 1995; Kotchenruther et al., 1999; L. Zhang et al., 2015):

$$\Delta FR(RH) = -(S_0/4) \times \left[T_a^2 \times (1 - A_C) \right]$$

$$\times \left[2 \times (1 - R_s)^2 \right]$$

$$\times \beta(RH) \times \tau_s - 4 \times R_s \times \tau_a, \qquad (3)$$

where S_0 is the solar constant, T_a is the atmosphere transmittance, A_C is the fractional cloud amount, R_s is the albedo of the underlying surface, $\beta(RH)$ is the upscattering fraction at a defined RH, and τ_s and τ_a are the optical thicknesses of the aerosol layer due to light scattering and light absorption, respectively, which can be expressed as follows (Kotchenruther et al., 1999):

$$\tau_{\rm s} = M \times \alpha_{\rm s} \times f({\rm RH}), \tau_{\rm a} = M \times \alpha_{\rm a},$$
 (4)

where M is the column burden of aerosol (unit: g m⁻²), α_s is the mass scattering efficiency (MSE), and α_a is the mass absorption efficiency (MAE). The direct radiative forcing is usually calculated with the assumption that the absorption enhancement is negligible in comparison to the aerosol scattering enhancement (Xia et al., 2023).

Hence, the dependence of ADRF on RH (i.e., $f_{RF}(RH)$) can be estimated by Eq. (5) (Chylek and Wong, 1995; Kotchenruther et al., 1999; L. Zhang et al., 2015):

$$\begin{split} f_{\rm RF}({\rm RH}) &= \frac{\Delta F_{\rm R}({\rm RH})}{\Delta F_{\rm R}({\rm dry})} \\ &= \frac{(1-R_{\rm s})^2 \times \beta({\rm RH}) \times \alpha_{\rm s} \times f({\rm RH}) - 2 \times R_{\rm s} \times \alpha_{\rm a}}{(1-R-{\rm s})^2 \times \beta({\rm dry}) \times \alpha_{\rm s} \times f({\rm dry}) - 2 \times R_{\rm s} \times \alpha_{\rm a}}, \quad (5) \end{split}$$

where the constant parameters used are $R_s = 0.15$ and $\alpha_a = 0.3 \text{ m}^2 \text{ g}^{-1}$ (Hand and Malm, 2007; Fierz-Schmidhauser et al., 2010). It should be noted that the assumed constant α_a might introduce some uncertainty in the calculated $f_{RF}(RH)$,

given the fact that the contribution of absorption by brown carbon was unknown, although the mass fraction of BC in TSP remained almost constant (i.e., 4.6 % \pm 1.1 %, Fig. S3) during the observation period. The parameter α_s was calculated by dividing $\sigma_{sca,\,525}$ in the dry condition by the mass concentration of PM_{2.5} (i.e., $\alpha_s = \sigma_{sca,\,525}/PM_{2.5}$). β could be calculated empirically from the measured HBF: $\beta = 0.0817 + 1.8495 \times HBF - 2.9682 \times HBF^2$ (Delene and Ogren, 2002).

3 Results and discussion

3.1 Overview of the aerosol optical hygroscopicity and PNSD measurements

Figure 1 displays the time series of the measured aerosol scattering coefficients, f(RH), PNSD, and the corresponding meteorological conditions and air pollutants during the study period. A sharp decrease in aerosol scattering coefficients and PM_{2.5}, accompanied by continuous excellent visibility over 20 km, was observed after 6 August, indicating a markedly cleaner environment during P2 in comparison to P1 in the summer of 2022 of Chongqing. This can largely be attributed to the reduction in anthropogenic emissions (e.g., NO₂ and CO but not SO₂) from limited outdoor activities influenced by the heatwaves in P2, as well as from the partial suspension of industries and transportation to alleviate the power shortage issue (Chen et al., 2024). Notably, the increased wind speed and enhanced mixing layer height (MLH) also enabled a more favorable atmospheric diffusion condition in P2, facilitating the dilution of surface air pollutants (Zhang et al., 2008). However, a higher mass concentration of SO₂ was observed in the P2 period, likely due to a surge in electricity demand and resulting higher emissions from power plants operating at almost full capacity during the heatwave (Su, 2021; Teng et al., 2022). Moreover, significant discrepancies in aerosol optical and hygroscopic properties were observed under different synoptic conditions (Table S2). Both HBF and SAE were higher during the P2 period, aligning with the smaller R_{eff} (Table S2). f(RH)was found to be relatively higher (p < 0.05) on heatwave days, with mean values of 1.61 ± 0.12 and 1.71 ± 0.15 during the P1 and P2 periods, respectively. In contrast, ALWC was more abundant during the normally hot P1 period than the heatwave-dominated P2 period. This is likely due to the fact that the derivation algorithm of ALWC utilized in this study (Kuang et al., 2018) is partly dependent on (e.g., positively correlated to) the dry aerosol scattering coefficient or, rather, the aerosol volume concentration in the dry condition (refer to Sect. S3 and Fig. S11 of the Supplement). The mean $\sigma_{sca, 525}$ for P2 was about 46.8% of that for the P1 period, and the corresponding mean level of ALWC was approximately 55.8 % of that for P1. This partly agrees with the stronger aerosol optical hygroscopicity, with a marginally higher $f_{\rm W}$ during the P2 period, highlighting a complex interaction between the optical enhancement and aerosol physic-ochemical properties.

The particle number size distribution data suggested that NPF events occurred on about half of the observation days (Fig. 1i), with an overall occurrence frequency of 52.4 % (Fig. S4a). This indicates that summer NPF events are rather frequent in Chongqing, being notably more common than those observed in other regions of the world, e.g., Beijing (16.7%, Deng et al., 2020; $\sim 20\%$, Wang et al., 2013), Dongguan (4 %, Tao et al., 2023), Hyytiälä (<40 %, Dada et al., 2017), and LiLLE (<20%, Crumeyrolle et al., 2023). Moreover, the frequent NPF events during heatwaves formed substantially ultrafine particles that contributed less to aerosol optical properties in comparison to large particles (Fig. S13), partially explaining the significantly lower levels of total scattering coefficients observed during the P2 period. It should be noted that the hourly $\sigma_{sca. 525}$ values during the P2 period were exclusively below 100 Mm⁻¹ (approximately the lowest 10th percentile of $\sigma_{sca, 525}$ data, regarded as the threshold value of relatively polluted cases; Fig. S2c), suggesting a much cleaner environment compared to the relatively polluted P1 period. Correspondingly, NPF events occurring during the relatively polluted P1 period (as detailed in Sect. 3.2) are defined as NPF_{polluted}, while cases during the cleaner and heatwave-dominated P2 period are classified as NPF_{clean}, HW.

3.2 Characteristics of NPF events in different periods

Aside from gaseous precursors (e.g., SO₂, volatile organic compounds), meteorological conditions also play a key role in the occurrence of NPF events. In brief, NPF events are more likely to appear under sunny and clean conditions (Bousiotis et al., 2021; Crumeyrolle et al., 2023; Deng et al., 2021; Wang et al., 2017). The backward trajectory analysis revealed that a southerly breeze was predominant during the study period (Fig. S4b). Although the surface wind vector slightly varied between the P1 and P2 periods, this consistency in air mass origins suggests that some other factors (e.g., changes in environmental conditions and emissions of gaseous precursors under heatwaves) could have played a crucial role in modulating NPF events. To further explore the characteristics of NPF events in different periods, the timeaveraged diurnal variations in meteorological parameters and air pollutant concentrations during both NPF events and nonevent days are presented in Fig. 2.

As stated in Sect. 3.1, NPF events during the P1 period tended to occur in relatively polluted environments compared to those of P2 NPF_{clean, HW} events, as evidenced by the frequent occurrence of $\sigma_{sca, 525} > 100 \, \mathrm{Mm^{-1}}$, increased air pollutant concentrations, and lower visibility levels during P1 (Table S2, Fig. 1). Additionally, the mean CS of the NPF_{polluted} events was above $0.015 \, \mathrm{s^{-1}}$ (Table S2), which could be considered "polluted" NPF cases (Shang et al., 2023). On P2 NPF_{clean, HW} days, the overall mean $\sigma_{sca, 525}$

was $33.2 \pm 11.7 \,\mathrm{Mm}^{-1}$, decreased by $68.0 \,\%$ (39.3 %) in comparison to that for P1 NPFpolluted days (P2 non-event days). In addition, the mean $PM_{2.5}$ concentration was even lower than $10.0 \,\mu \text{g m}^{-3}$, and the corresponding visibility level was almost maintained at 30 km (Fig. 1e). All the above implies that the P2 NPF_{clean, HW} events were generally accompanied by a much cleaner environment. It is notable that the increase in SO₂ concentration after 09:00 LT (Fig. 2d), along with the significant decrease in PM_{2.5} mass loadings after 08:00 LT during P1 NPF_{polluted} events (Fig. 2b), likely favored the occurrence of NPF events. The higher gas-phase sulfuric acid (i.e., H₂SO₄, as estimated with the UVB and SO₂ concentration; Lu et al., 2019; Sect. S4) on the same NPF days (Fig. 2f) further suggests that sulfuric acid concentration was a critical factor for the occurrence of P1 NPF_{polluted} events.

The diurnal evolutions of meteorological conditions (e.g., T, RH, MLH) for NPF events were distinct between the P1 and P2 periods, although relatively insignificant differences were observed for both NPF days and non-event days within the same period (Fig. 2). This likely suggests that meteorological factors might not be the predominant determining factor of NPF occurrence during the heatwaves of the summer of 2022 in urban Chongqing, while NPF could be accompanied by quite different meteorological conditions depending on gaseous precursors and pre-existing condensation sinks. For instance, the NPF_{clean, HW} events were typically cleantype NPF, characterized by lower background aerosol loading, higher temperature, and favorable atmospheric dispersion capacity with the higher MLH. However, it is reported that excessive heat can increase the evaporation rate of critical acid-base clusters during the nucleation process and reduce the stability of initial molecular clusters (Bousiotis et al., 2021; Kurtén et al., 2007; Zhang et al., 2012), in line with a recent study reporting that NPF events were weaker during heatwaves in a Siberian boreal forest due to the unstable clusters (Garmash et al., 2024). On the other hand, the emission rate of biogenic VOCs (BVOCs, e.g., isoprene, monoterpene) from nearby plants and trees would decrease when temperature exceeded around 40 °C (Guenther et al., 1991; Pierce and Waldruff, 1991), despite the fact that BVOCs play a key role in the nucleation mechanism of NPF (Wang et al., 2017; Zhang et al., 2004). Hence, the even higher temperature (e.g., $T > 40^{\circ}$) likely suppressed the nucleation processes and the subsequent growth of nucleation mode particles on P2 non-event days (Fig. S6b2), in spite of higher concentrations of SO_2 and H_2SO_4 .

To further investigate the effect of heatwaves on NPF events, the diurnal variations in PNSD, $R_{\rm eff}$, and particle mode diameter ($D_{\rm mode}$) are shown in Fig. S6. Aerosol number and volume concentrations, as well as $R_{\rm eff}$, for different modes are illustrated in Figs. S7–S8, and the relationship between temperature and the duration of NPF events is displayed in Fig. S9. Distinct particle size distributions were observed for different NPF event days.

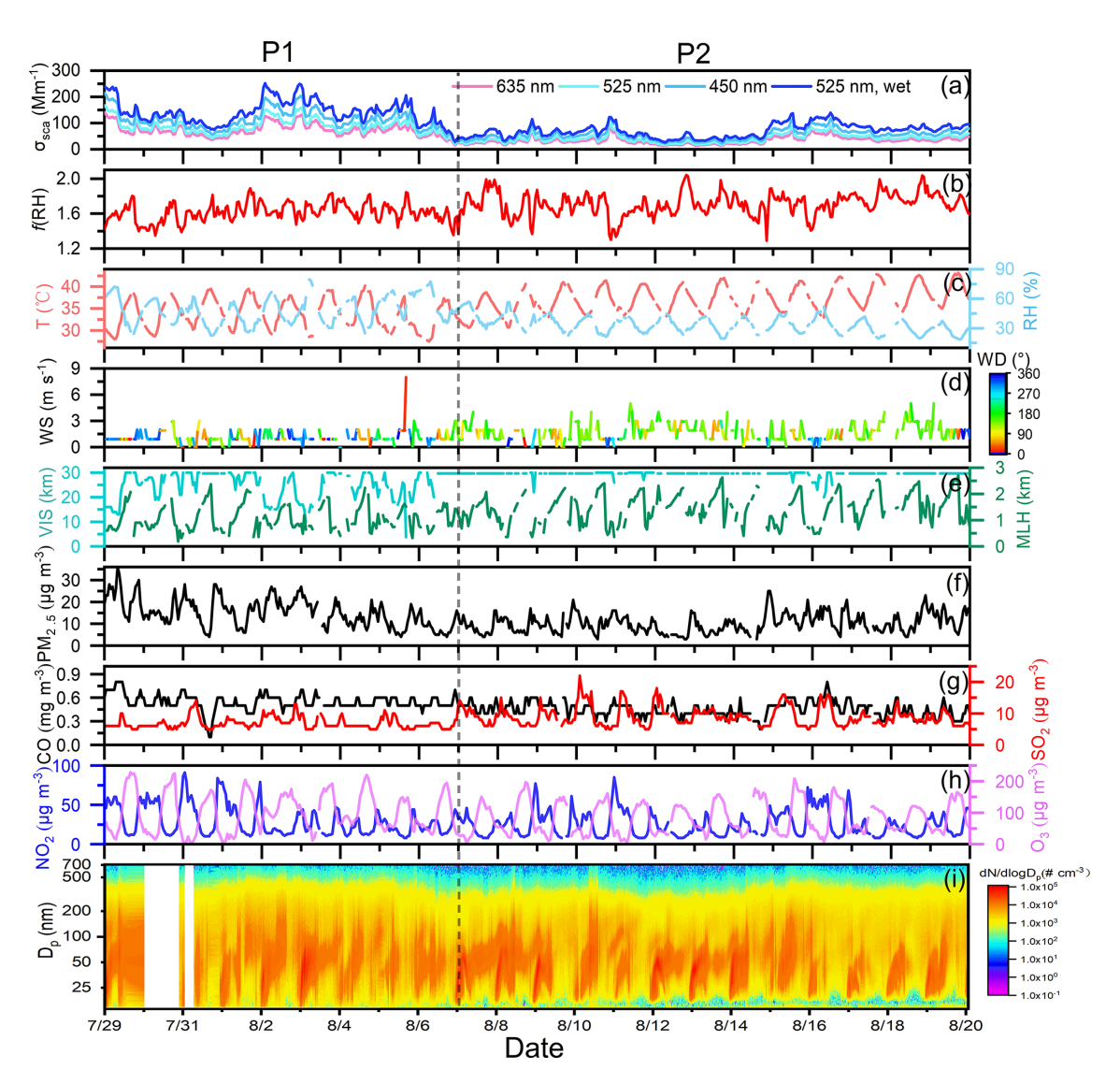


Figure 1. Time series of the measured aerosol scattering coefficients, f(RH), meteorological conditions, air pollutants, and particle number size distribution during the study period.

While the number concentrations of Aitken mode particles (NAit.) were comparable during NPF days of both periods, the corresponding number concentration of nucleation mode particles (N_{Nuc.}) was significantly higher on P1 NPF_{polluted} days $(1880.8 \pm 2261.5 \,\mathrm{cm}^{-3})$ than on P2 NPF days $(1132.0 \pm 1333.5 \,\mathrm{cm}^{-3})$ (Figs. 1i, S7). Different from that of the P1 NPF_{polluted} cases, the P2 NPF_{clean, HW} event did not start from the minimum size, and the reduced $N_{\text{Nuc.}}$ during the P2 period is likely attributable to the influence of transport on the local nucleation and growth processes (Fig. S4; Cai et al., 2018; Lee et al., 2019). Namely, some nucleation mode particles transported from upwind regions or from the mixing layer downwards had undergone atmospheric aging and thereby a certain degree of growth upon arrival (Cai et al., 2018; Lai et al., 2022; Platis et al., 2016), resulting in relatively lower concentrations of smaller-sized

particles than in the case of locally formed particles. However, the local formation of sub-25 nm particles and the continuous growth process were still distinctly observed under heatwaves (Figs. 1i, S6, S15). The NPF events under heatwaves usually initiated earlier (Fig. S9), with $N_{\text{Nuc.}}$ in P2 NPF_{clean, HW} cases peaking about an hour earlier in comparison to NPF_{polluted} days (Fig. S8a). D_{mode} on P2 NPF_{clean, HW} days also reached its minimum earlier than on P1 NPF_{polluted} days (Fig. S6). Since the sunrise and sunset times did not significantly vary within the study period (i.e., less than a half-hour discrepancy), heatwaves likely provided more favorable conditions (e.g., enhanced volatile gaseous emissions, low RH; Bousiotis et al., 2021; Hamed et al., 2007; Wang et al., 2024) for the occurrence of NPF events in urban Chongqing. This is supported by the earlier start time of NPF_{clean, HW}, corresponding to higher temperature ranges

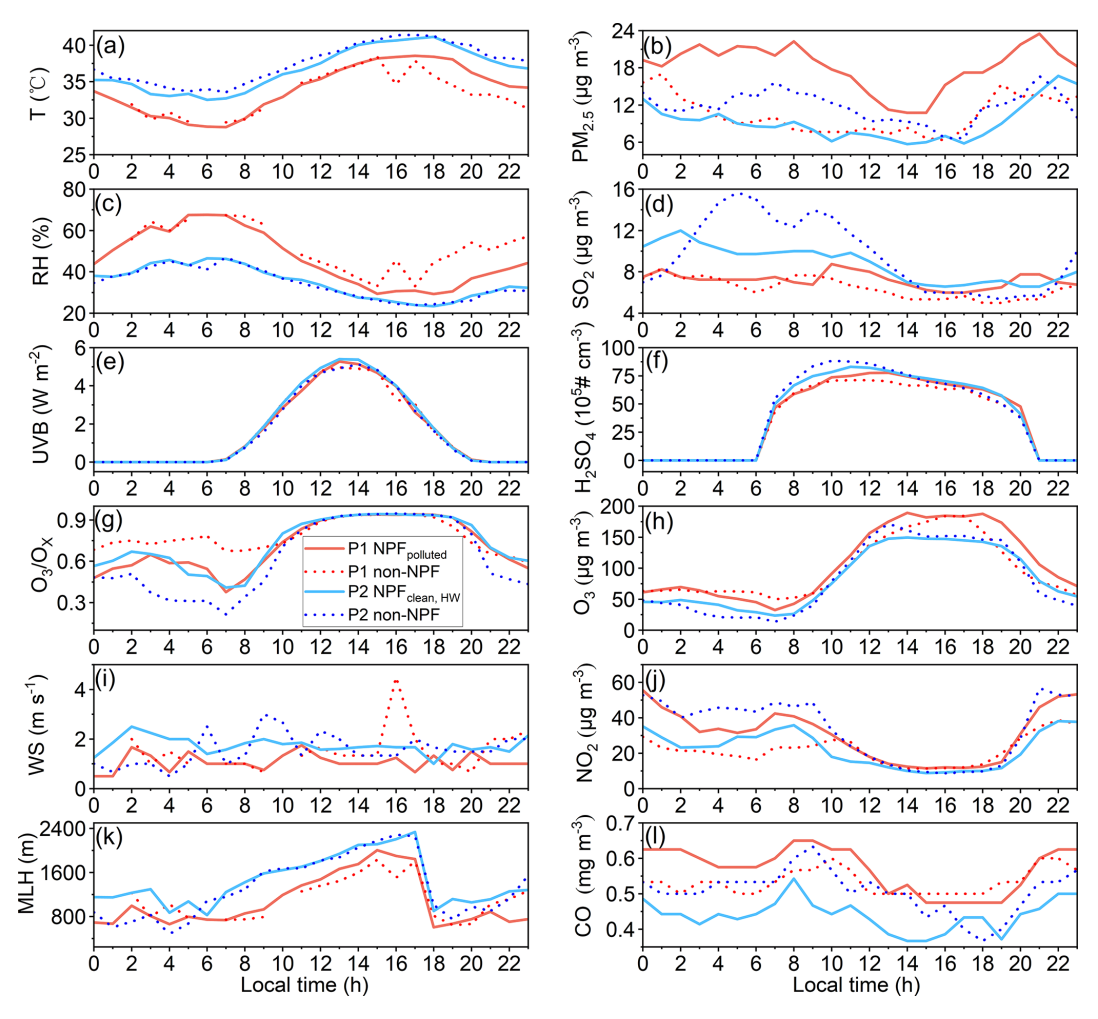


Figure 2. Diurnal variations in temperature (**a**), PM_{2.5} mass loading (**b**), RH (**c**), SO₂ (**d**), UVB (**e**), H₂SO₄ (**f**), O₃/O_X (**g**), O₃ (**h**), WS (**i**), NO₂ (**j**), MLH (**k**), and CO (**l**) during P1 (red) and P2 (blue) NPF days (solid line), as well as the corresponding non-event days (dashed line).

(Fig. S9). Furthermore, the end time of subsequent particle growth during the P2 period was even later (i.e., $\sim 21:00$ LT) than that of P1 cases (Fig. S9). Given that the growth rates of new particles were generally lower during P2 NPF_{clean, HW} events (Table S2), these explosively formed new particles could persist longer in the warmer atmosphere and probably underwent aging processes with a relatively higher oxidation degree. This is supported by the commonly higher ratios of secondary organic carbon (SOC) to organic carbon (OC) (i.e., SOC/OC > 0.5) during the NPF_{clean, HW} days (Fig. S3b). In addition, aerosol $R_{\rm eff}$ was significantly smaller on the NPF_{clean, HW} days under heatwave conditions. R_{eff} and D_{mode} were maintained at nearly the same level below/approaching 50 nm during the subsequent growth on the P2 NPF_{clean. HW} days, while $R_{\rm eff}$ was generally above 50 nm and larger than D_{mode} for both P1 NPF_{polluted} cases and nonevent days (Fig. S6). The diurnal patterns of aerosol volume concentrations for different size modes were similar to

those of aerosol number concentrations during NPF events (Fig. S8b1–b3). However, $R_{\rm eff}$ of both Aitken mode particles ($R_{\rm Ait.}$) and accumulation mode particles ($R_{\rm Acc.}$) was smaller during P2 NPF_{clean, HW} events than during P1 NPF_{polluted} events (Fig. S8c2–c3), which may further influence size-dependent aerosol optical and hygroscopic properties (e.g., $\sigma_{\rm sca}$, 525, HBF, SAE, $f({\rm RH})$). The decrease in $R_{\rm Ait.}$ and $R_{\rm Acc.}$ during heatwaves can be attributed to three factors: (1) evaporation of the outer layer of particles and unstable clusters due to heatwaves (Bousiotis et al., 2021; Cusack et al., 2013; Deng et al., 2020; Garmash et al., 2024; Li et al., 2019), (2) lower FR and GR of particles under cleaner-environment conditions (Table S2), and (3) reduced emissions of larger primary particles during the P2 period.

3.3 Characteristics of the aerosol optical and hygroscopic properties on different types of NPF days

Diurnal variations in the aerosol optical and hygroscopic parameters during different NPF days are shown in Fig. 3, and the corresponding results for non-event days are shown in Fig. S10. Generally, $\sigma_{\text{sca}, 525}$ possessed a similar bimodal diurnal pattern to that of the accumulation mode aerosol volume concentration ($V_{Acc.}$) (Fig. S8b3), as supported by the positive correlation between $\sigma_{sca, 525}$ and SMPS-measured aerosol volume concentration (Fig. S12). This is also consistent with Mie theory, with a stronger increase in the scattering efficiency for accumulation mode particles (Titos et al., 2021). The diurnal pattern of $\sigma_{\text{sca.}}$ 525 also varied distinctly between different NPF days. Specifically, a minor peak in $\sigma_{\rm sca. 525}$ around 12:00 LT (Fig. 3a) was influenced by the newly formed particles during P2 NPF_{clean, HW} events, which contributed more significantly to the aerosol number and volume concentrations within 100 nm size ranges in markedly clean environments (Fig. S5c1, c2). Instead of a noontime peak, $\sigma_{\text{sca, 525}}$ was observed with an early peak around the morning rush hours, and a maximum value similarly occurred at nighttime on P1 NPF_{polluted} days.

Both HBF and SAE on P2 NPF_{clean, HW} days were significantly higher than during P1 NPFpolluted cases (Fig. 3c, e), largely due to the smaller $R_{\rm eff}$ observed during the heatwavedominated period (Table S2). Moreover, the correlation between HBF (or SAE) and particle size in each mode was weaker on NPF days than on non-event days, especially for NPF_{clean, HW} days (Fig. S14). The strongest negative correlation was found between HBF and $R_{\rm eff}$ of the accumulation mode in comparison to other modes, highlighting that HBF is more sensitive to the size distribution of accumulation mode particles (Collaud Coen et al., 2007). Given that NPF would largely enhance the abundance of both nucleation and Aitken mode aerosols (Fig. S7), no significant variation in HBF was observed during the daytime due to the weakened correlation between HBF and R_{Acc.} of NPF events. SAE is commonly used as an indicator of particle size distribution, almost decreasing monotonously with the increase in aerosol size within 1 µm (Kuang et al., 2017, 2018; Luoma et al., 2019). Accordingly, SAE decreased over the morning and evening rush hours, when coarse particles (e.g., aged particles, road dust, automobile exhaust) generated during anthropogenic activities were present, accompanied by an increase in CO, which is taken as a proxy for primary emissions (Fig. 21) (Yarragunta et al., 2021). In contrast, the abundant ultrafine particles formed during NPF events led to a continuous increase in SAE during the day.

f(RH) exhibited a similar diurnal pattern on P1 and P2 NPF days (Fig. 3b). During the daytime, f(RH) remained relatively stable and gradually increased until peaking around 16:00–18:00 LT, with a generally higher f(RH) particularly after 15:00 LT during P2 NPF_{clean, HW} days than during

P1 cases. The insignificant fluctuations in relatively lower f(RH) levels before noon could be attributed to the continuous development of the mixing layer (Fig. 2k), leading to efficient mixing of particles in the nocturnal residual layer with anthropogenic emissions near the ground. Additionally, photochemical reactions in the afternoon facilitated the formation of more hygroscopic secondary aerosols with a higher oxidation level (Liu et al., 2014; R. Zhang et al., 2015). The diurnal patterns of O_3 and the O_3/O_X ratio (i.e., an indicator of atmospheric oxidation capacity, where $O_X = O_3 + NO_2$, Tian et al., 2021) also showed similar trends (Fig. 2g, h). The presence of black carbon (BC) mixed with organic compounds (e.g., from traffic emissions and residential cooking activities) explained the rapid decrease in f(RH) during the evening rush hours (Liu et al., 2011). Furthermore, the daily mean f(RH) for NPF days was higher than that of non-event days (Table S2), particularly after the end of NPF events around 12:00 LT. Given that newly formed particles were too small to significantly impact the total light scattering (Fig. S11a), this indicates that the atmospheric conditions conducive to the occurrence of NPF may promote further growth (e.g., via intensified/prolonged photooxidation or atmospheric aging processes) of pre-existing particles and newly formed ones, partly contributing to enhanced aerosol optical hygroscopicity, as indicated by the concurrent variations in ALWC and $f_{\rm W}$ in urban Chongqing during the hot summer (Asmi et al., 2010; Wang et al., 2019; Wu et al., 2016). The diurnal pattern of ALWC closely mirrored the variation in $\sigma_{\text{sca}, 525}$, while f_{W} followed a similar evolution to f(RH). This suggests that ALWC was more sensitive to changes in the aerosol volume concentration, as determined by the corresponding retrieval algorithm (Kuang et al., 2018). f_W levels were slightly higher during NPF days in comparison to those on non-event days (Table S2). This difference was more pronounced in the afternoon of NPF days (e.g., even exceeding 50 %; Fig. 3f), verifying the enhancement of aerosol hygroscopicity during the subsequent growth and atmospheric aging of both pre-existing and newly formed particles.

Heatwave-induced divergent changes in aerosol optical hygroscopicity

To further explore the impacts of heatwaves on f(RH) during diverse NPF events, data mainly within the time window of 08:00-22:00 LT (i.e., typically covering the complete process of NPF and subsequent growth, while excluding higher-RH conditions at night) were utilized for the following discussion.

Although ultrafine particles exhibited higher number concentrations during the study period, accumulation mode particles dominated the aerosol volume concentration and contributed predominantly to the total light scattering (Figs. S7, S13). A positive correlation between f(RH), $R_{\rm eff}$, and the volume fraction of accumulation mode particles (VF_{Acc.})

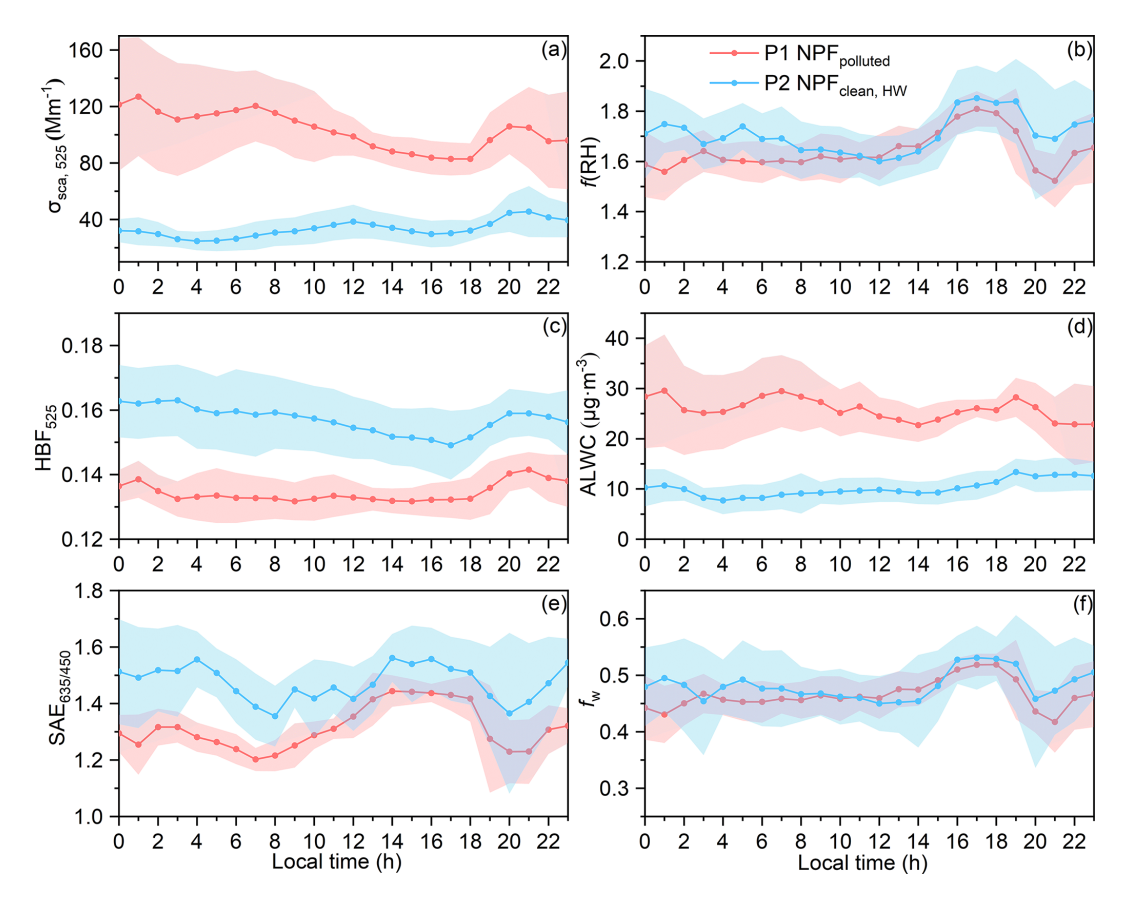


Figure 3. Diurnal variations in $\sigma_{\text{Sca}, 525}$ (a), f(RH) (b), HBF_{525} (c), ALWC (d), $\text{SAE}_{635/450}$ (e), and f_{W} (f) on NPF days during P1 (red line) and P2 (blue line) periods. The shaded areas represent the corresponding $\pm 1\sigma$ standard deviations.

was found on non-event days (Fig. 4c-d), when the aerosol size distribution was undisturbed by newly formed ultrafine particles and the corresponding VF_{Acc.} was maintained at a high level of approximately 0.95 (Fig. 4a-b). The notably positive correlation between f(RH) and R_{eff} could be linked to the secondary formation of hygroscopic particles within the accumulation mode, primarily via photochemical reactions, and further intensified by heatwaves during the nonevent day, particularly in the P2 period (Gu et al., 2023; Liu et al., 2014; R. Zhang et al., 2015; Zhang et al., 2024). Consequently, f(RH) at a specific R_{eff} was generally higher during the P2 period in comparison to that of P1 (Fig. 4c-d), also with high f(RH) levels observed for smaller-size cases of $R_{\rm eff}$ < 110 nm under some extremely high temperature conditions $(T>40^\circ)$, as highlighted by the dashed red circle in Fig. 4d). The higher SOC / OC on P2 non-event days further demonstrated the stronger secondary aerosol formation in comparison to P1 non-event days (Fig. S3b).

Nevertheless, f(RH) was almost independent of the two parameters (i.e., $R_{\rm eff}$ and $VF_{\rm Acc.}$) during NPF events (Fig. 4e–f). This is mainly due to the explosive formation of ultrafine particles and their subsequent growth on NPF days, significantly altering aerosol size distributions and inducing large fluctuations in NF_{Acc.} and VF_{Acc.} compared with non-

event days, especially during the P2 period (as shaded in Fig. 4a-b). Therefore, characterizing f(RH) by the corresponding $R_{\rm eff}$ of aerosol populations was no longer applicable. Alternatively, SAE was commonly used to estimate or parameterize f(RH) (Titos et al., 2014; Xia et al., 2023; Xue et al., 2022), in line with the similar diurnal patterns of f(RH) and SAE observed in this study. Figure 5 demonstrates a significantly positive correlation between f(RH)and SAE during NPF days in comparison to non-event days, with a similar slope of approximately 0.65, suggesting the consistent variation in f(RH) with SAE across both periods. As larger particles contributed more to aerosol volume concentrations (Fig. S5), the decrease in SAE also corresponded to an increase in $\sigma_{sca. 525}$ (Fig. 5a3, b3). Given that larger $\sigma_{\rm sca, 525}$ values typically indicate the condition of higher aerosol loading, f(RH) increased with SAE, whereas it decreased with $\sigma_{\rm sca.~525}$ or rather, the pollution level, during NPF days. The cleaner environment of the P2 period may further favor the occurrence of NPF events. Both f(RH) and SAE exhibited a higher level on P2 NPF_{clean, HW} days (as shown by the dashed lines in Fig. 5), probably due to the following two aspects. One is related to the smaller aerosol $R_{\rm eff}$ (with a larger SAE) due to the lower FR and GR, likely influenced by the evaporation of newly formed unstable clusters

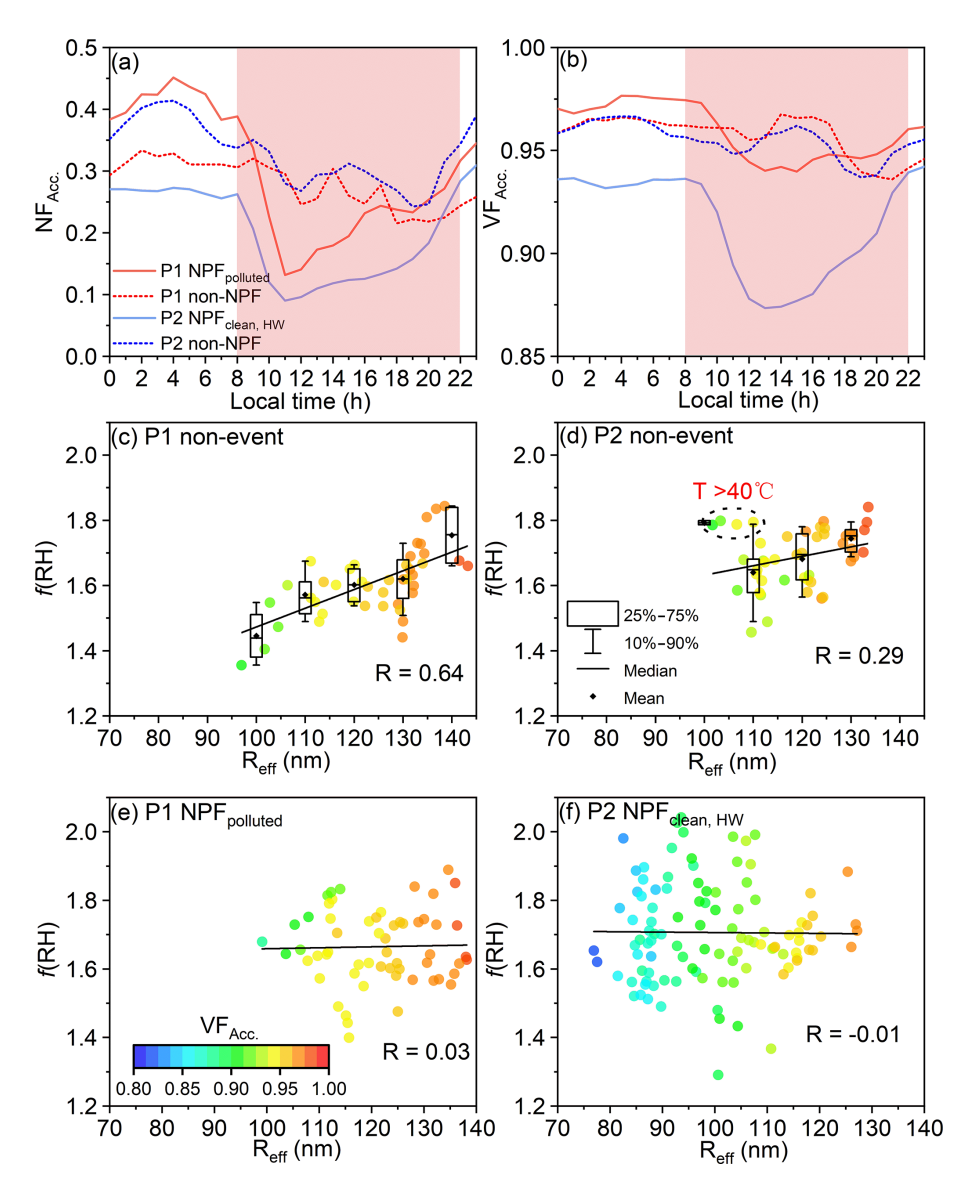


Figure 4. Diurnal variations in (a) the number fraction (NF_{Acc.}) and (b) volume fraction of accumulation mode particles (VF_{Acc.}) on P1 (red) and P2 (blue) NPF days (solid line) and non-event days (dashed line). The time window of $08:00-22:00\,LT$ is shaded in red. The relationship of f(RH) with R_{eff} and VF_{Acc.} (as indicated by the colored dots) on P1 (c) and P2 non-event days (d) and on P1 (e) and P2 (f) NPF days during the $08:00-22:00\,LT$ time window.

and particle coatings under heatwaves (Bousiotis et al., 2021; Cusack et al., 2013; Deng et al., 2020) during the subsequent growth of aerosols. Secondly, the higher temperature was normally associated with stronger photochemical oxidation, which could intensify the formation of secondary aerosol components with a higher hygroscopicity (Asmi et al., 2010; Gu et al., 2023; Liu et al., 2014; Wu et al., 2016; R. Zhang et al., 2015; Zhang et al., 2024). This is further supported by the slightly higher levels of UVB (P1: $2.6 \pm 1.9 \, \mathrm{W \, m^{-2}}$ versus P2: $2.7 \pm 2.0 \, \mathrm{W \, m^{-2}}$) and O_3/O_X (P1: 0.81 ± 0.17 versus P2: 0.82 ± 0.17) during P2 heatwave days, also in line with a recent study which demonstrated that heatwaves affected secondary organic aerosol (SOA) formation and ag-

ing by accelerating photooxidation in Beijing (Zhang et al., 2024).

It is worth noting that f(RH) did not show a consistently higher level after the NPF_{clean, HW} occurrence during the P2 period, and it was slightly higher within the first few hours of NPF occurrence (i.e., $\sim 12:00-15:00\,LT$) on P1 NPF_{polluted} days (Fig. 3b). In fact, aerosol optical hygroscopicity does not fully correspond to the bulk hygroscopicity, primarily determined by aerosol chemical components, and the variability in aerosol optical features also plays a key role in f(RH). Hence, the size dependency of aerosol optical properties should be considered. The size-resolved $\sigma_{sca, 525}$ distribution and size-resolved cumulative frequency distribution

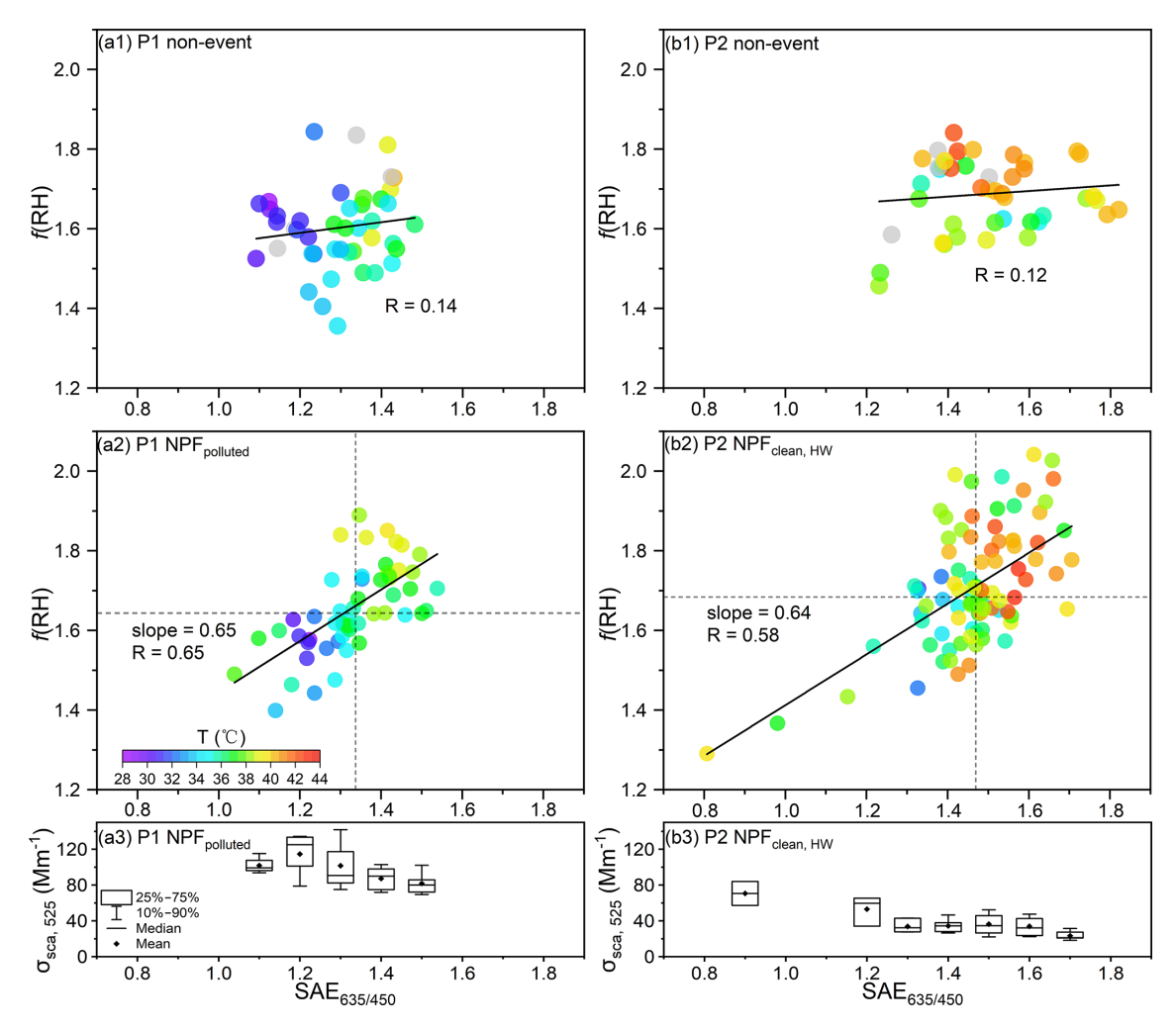


Figure 5. The relationship between f(RH) and $SAE_{635/450}$, as well as temperature (as indicated by the color of the dots; missing values are represented in gray), on P1 non-event days (**a1**) and NPF_{polluted} days (**a2**) during the 08:00–22:00 LT time window. The vertical (horizontal) dashed line represents the median value of $SAE_{635/450}$ (f(RH)). (**a3**) The corresponding $\sigma_{sca, 525}$ under different $SAE_{635/450}$ levels on P1 NPF_{polluted} days. (**b1–b3**) The same but for the P2 period.

(CFD) of $\sigma_{sca. 525}$ over different NPF days were calculated using Mie theory, with good agreement between the theoretically calculated and measured $\sigma_{\text{sca}, 525}$ values ($R^2 = 0.99$). As shown in Figs. S11a and S13, new particles must grow into the accumulation mode size at least before they can exert a significant influence on the total scattering coefficient. The critical sizes corresponding to the cumulative frequency of 50 % in $\sigma_{sca, 525}$ were 358.7 and 333.8 nm on P1 and P2 NPF days, respectively. This indicates that relatively smaller particles – including the newly formed and grown particles mixed with pre-existing and aged particles - contributed a slightly higher portion to $\sigma_{\text{sca}, 525}$ on P2 NPF_{clean, HW} days, while $\sigma_{sca, 525}$ was mainly contributed by larger particles on P1 NPF_{polluted} days. Nevertheless, Mie theory suggests that these smaller particles generally have a weaker enhancement in total scattering after hygroscopic growth in comparison to larger size particles (Collaud Coen et al., 2007, Fig. S11a).

Consequently, the changes in aerosol optical and hygroscopic properties necessitate consideration of both aerosol optical and chemical characteristics during different NPF events. Newly formed ultrafine particles contributed less to aerosol optical properties, resulting in lower f(RH) during the initial hours of P2 NPF_{clean, HW} events compared to P1 $NPF_{polluted}$ events (Fig. 3b), as evidenced by smaller R_{eff} for P2 NPF_{clean, HW} events (Fig. S6). In contrast, the growth of pre-existing and newly formed particles into larger sizes would subsequently affect bulk aerosol optical properties, which was evidenced by the enhancement in the aerosol extinction coefficient observed after NPF occurrence in a recent study (Sun et al., 2024). Specifically, particles could undergo a longer and more intensified photochemical aging process during NPF_{clean, HW} days, as influenced by persistent heatwaves, which facilitated the secondary formation of hygroscopic aerosols and jointly contributed to higher f(RH) after 15:00 LT (Fig. 3b).

3.5 *f*(RH)-induced changes in aerosol direct radiative forcing

The changes in f(RH) have significant implications for aerosol direct radiative forcing. Despite considerably lower $\sigma_{\rm sca,\ 525}$ results during heatwaves, the corresponding mean $f_{\rm RF}(RH)$ levels, particularly for P2 NPF_{clean, HW} days, were higher than those of the P1 cases (Fig. 6a). A robust positive correlation ($R^2=0.68$) was observed between f(RH) and the aerosol radiative forcing enhancement factor, $f_{\rm RF}(RH)$ (Fig. 6b). This is likely due to the enhanced $f_{\rm RF}(RH)$ with the larger forward scattering ratio β , or rather higher HBF for smaller particle sizes, as supported by a generally negative correlation between $f_{\rm RF}(RH)$ and $r_{\rm eff}$. Specifically, the highest $r_{\rm RF}(RH)$ value of $r_{\rm RF}(RH)$ and sobserved on P2 NPF_{clean, HW} days, characterized by the highest $r_{\rm RH}(RH)$ and smallest $r_{\rm eff}$ (i.e., highest HBF) of the entire study period.

The definition of $f_{RF}(RH)$ in Eq. (5) implies its dependence on both f(RH) and HBF-derived $\beta(RH)$ and β (dry), or, more precisely, the ratio of HBF₅₂₅, RH / HBF₅₂₅. The mean HBF_{525, RH} was generally larger than HBF₅₂₅ in this study, specifically with the HBF_{525, RH} / HBF₅₂₅ ratios centered around 1.8, and even approached 2.5 on P2 NPF_{clean, HW} days (Fig. 6c, Table S2). This could differ from classical Mie theory with its spherical-particle premise; i.e., the observed light backscattering was enhanced after hydration, likely as a result of the evolution in particle morphology that significantly influences its optical properties (Mishchenko, 2009). Additionally, the predominant organic components, when heterogeneously mixed with diverse chemical compositions (e.g., inorganics and black carbon), likely introduced the heterogeneity in aerosol hygroscopicity (Yuan and Zhao, 2023), which may alter particle morphology and thereby optical properties upon water uptake (Giordano et al., 2015; Tan et al., 2020; Tritscher et al., 2011). The efficient evaporation of organic coatings under extremely hot conditions could also contribute to the change in particle morphology (e.g., non-spherical irregular shapes) upon humidification, as evidenced by a recent study that reported that high-temperature conditions could accelerate the evaporation rate of SOA (Li et al., 2019). Given that the backward scattering intensity of non-spherical particles is suggested to be much larger than that of their spherical counterparts at scattering angles between 90 and 150° (Mishchenko, 2009; Yang et al., 2007) and that the HBF-derived asymmetry parameter (g) normally correlates positively with the aerosol forward scattering (Andrews et al., 2006; Marshall et al., 1995), the generally smaller g_{RH} results (in comparison to g) confirmed the decrease (increase) in forward (backward) light scattering after water uptake (Fig. S11c), likely implying a change in the morphological structure of particles. This is particularly evident for P2 NPF_{clean, HW} days, during which a much lower level of g_{RH} was observed (Fig. S11c). Another possible reason is the distinct size dependences of both light scattering and backscattering efficiencies (Fig. S11a), with much more significant enhancements in the backscattering efficiency and thereby HBF, specifically of accumulation mode particles after hygroscopic growth (Fig. S11b). As reflected by the Mie model, although the abundant newly formed particles were generally optically insensitive (e.g., below 100 nm), their contributions to $\sigma_{sca, 525}$ and especially to $\sigma_{\rm bsca, 525}$ could be amplified upon humidification (Fig. S11b). Moreover, the shift of the size distribution towards larger accumulation mode particles could also result in a significant elevation in HBF₅₂₅, RH / HBF₅₂₅ ratios, especially under the condition of a smaller-mode diameter and narrower distribution of ultrafine-mode particles (e.g., during NPF events) (Fig. S16a1-b2 for the theoretical sensitivity tests of Sect. S9 in the Supplement). Furthermore, the HBF_{525 RH} / HBF₅₂₅ ratio exhibited a significant positive correlation with the real part of the complex refractive index (n) of bulk aerosols (Fig. S17), and n tends to increase with the aging process of organic species (Moise et al., 2015; G. Zhao et al., 2021). In this sense, the evolution of both aerosol size distribution patterns and chemical compositions, combined with the heterogeneity in aerosol hygroscopicity, could potentially change particle morphology and optical properties (e.g., complex refractive index and elevated HBF_{525. RH}), particularly during heatwave-influenced $NPF_{clean. HW}$ days, characterized by the smallest aerosol R_{eff} $(102.8 \pm 12.4 \,\mathrm{nm})$ (Fig. S6), lowest number concentration $(1897.0 \pm 680.8 \,\mathrm{cm}^{-3})$ and fraction (0.20 ± 0.10) of accumulation mode particles, intensified photooxidation, and a higher SOC / OC ratio. The higher HBF_{525, RH} / HBF₅₂₅ ratios increased the HBF-derived $\beta(RH)/\beta(dry)$ levels, in combination with the elevated f(RH), further resulting in the highest $f_{RF}(RH)$ observed during P2 NPF_{clean, HW} events. Given that previously observed HBF_{525, RH} was typically lower than HBF₅₂₅ (Titos et al., 2021; Xia et al., 2023; L. Zhang et al., 2015), the mean $f_{RF}(RH)$ results of this study $(f_{RF}(85\%) = 2.05 \pm 0.24)$ were significantly higher than those observed in the Yangtze River Delta ($f_{RF}(85\%)$ = 1.5, L. Zhang et al., 2015), the North China Plain ($f_{RF}(80\%)$ $= 1.6 \pm 0.2$, Xia et al., 2023), and some other regions in the world (Titos et al., 2021, Fig. 6d). It should be noted that the reported $f_{RF}(RH)$ for the UGR site (Spain) was even higher, likely due to the higher R_s and α_s used in the derivation of $f_{RF}(RH)$ in that area (Titos et al., 2021).

A recent study has indicated that continuous reduction in $PM_{2.5}$ mass loadings can increase the net solar radiation, thereby promoting NPF events (S. Zhao et al., 2021). Given the complexity and dynamic evolution of the atmospheric environment, these can further alter the intrinsic properties of aerosol particles (e.g., f(RH), HBF, morphology), potentially feeding back into aerosol–radiation interactions. Our findings suggest that NPF days may possess a relatively

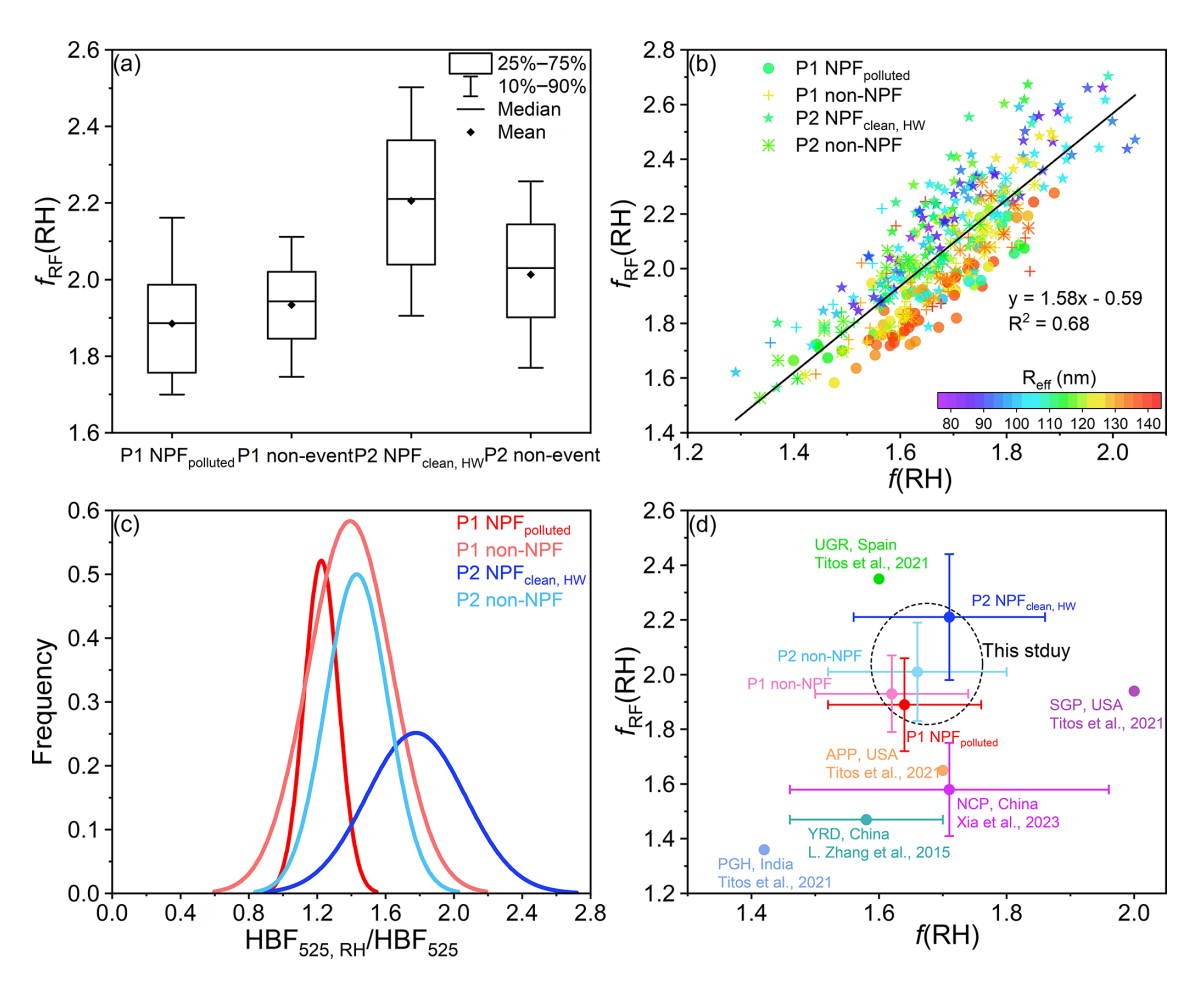


Figure 6. (a) The boxplot of $f_{RF}(RH)$ during P1 and P2 NPF event and non-event days. (b) The relationship between $f_{RF}(RH)$ and f(RH), as colored by the corresponding R_{eff} , during P1 and P2 NPF and non-event days (shown with different symbols). (c) Occurrence frequency of the HBF₅₂₅, RH / HBF₅₂₅ ratios during P1 and P2 NPF and non-event days. (d) The mean $f_{RF}(RH)$ under different f(RH) levels (the error bars represent ± 1 standard deviation corresponding to $f_{RF}(RH)$ and f(RH)), along with the reported $f_{RF}(RH)$ and f(RH) data for other regions in the world.

higher aerosol optical hygroscopicity in rather hot environments, e.g., the basin area and tropical regions. Meanwhile, NPF serves as a crucial secondary transformation process in the atmosphere (Zhu et al., 2021). The favorable atmospheric diffusion capability ensured the mixing of newly formed particles into the upper boundary layer, where it is colder and more humid compared to near the surface during heatwaves (Jin et al., 2022). Hence, the enhancement of aerosol optical hygroscopicity during the subsequent growth and aging of both pre-existing and newly formed particles possibly exacerbates secondary pollution and even triggers haze events (Hao et al., 2024; Kulmala et al., 2021). On the other hand, a large number of studies have demonstrated that the new particles with higher hygroscopicity could contribute more to the activation of CCN (Ma et al., 2016; Ren et al., 2021; Rosati et al., 2022; Sun et al., 2024; Wu et al., 2015), thereby modulating aerosol-cloud interactions and further the global climate (Fan et al., 2016; Merikanto et al., 2009; Westervelt et al., 2013). Additionally, the simultaneous decrease in aerosol effective radius and possibly evaporation-induced non-spherical particle morphology further enhance the aerosol direct radiative forcing enhancement factor, potentially amplifying the cooling effect mainly caused by light scattering aerosols. This highlights the need for further indepth exploration of aerosol radiative impacts under heatwaves with a changing climate, given the continuous reductions in anthropogenic emissions and more intense emissions of biogenic origins with global warming. Moreover, more detailed information on the evolution of particle morphology with the changing environment (e.g., varied temperature and RH) would enrich insights into aerosol radiative forcing.

4 Conclusions and implications

A rare heatwave event raged throughout urban Chongqing of southwest China in the summer of 2022, which signif-

icantly influenced aerosol physicochemical properties and atmospheric processes (e.g., NPF and subsequent growth). Concurrent measurements of aerosol optical and hygroscopic properties, PNSD, and bulk chemical compositions were conducted to explore the mechanisms behind the variations in aerosol optical hygroscopicity during different NPF days under diverse weather conditions.

Although the air masses and the occurrence frequencies of NPF events were similar during different periods, NPF events exhibited distinct characteristics during the normally hot (P1, relatively polluted) and heatwave-dominated (P2, quite clean) periods. NPF_{polluted} within the P1 period was favored by the decrease in background aerosol loading and the higher abundance of H₂SO₄. NPF_{clean, HW} events, which occurred during the heatwave P2 period, were observed with lower CS, CoagS, FR, and GR, as well as smaller Reff and D_{mode}, compared to P1 NPF_{polluted} cases. According to the measured PNSDs, P1 NPF_{polluted} events were mainly driven by local growth, while NPF_{clean}. HW events may be largely affected by transport under heatwaves. In comparison to P1 NPF_{polluted} events, NPF_{clean, HW} occurred approximately 1 h earlier, and the subsequent growth was longer during P2, likely intensifying the photochemical oxidation and prolonging atmospheric aging processes under heatwaves, thereby modulating the evolution of aerosol size distributions and chemical characteristics differently. Furthermore, significant differences in aerosol optical and hygroscopic properties were observed between the normally hot and heatwavedominated NPF days. The newly formed and grown particles mixed with pre-existing aerosols contributed a minor $\sigma_{\rm sca. 525}$ noontime peak that occurred on the much cleaner P2 NPF_{clean, HW} days, while $\sigma_{sca, 525}$ peaked earlier, around the morning rush hours on P1 NPFpolluted days. HBF and SAE were significantly higher on P2 NPF_{clean, HW} days, primarily due to the smaller $R_{\rm eff}$ for heatwave-influenced NPF_{clean, HW} cases. f(RH) remained relatively stable during the daytime of NPF days and peaked around 16:00-18:00 LT. Specifically, aerosol optical hygroscopicity was observed to be higher during the subsequent growth and aging of both preexisting particles and newly formed ones on P2 NPF_{clean, HW} days than that for P1 NPF_{polluted} days, which aligned with the higher $f_{\rm W}$ levels.

Compared with non-event cases, the daily mean f(RH) levels were generally higher on NPF days in the hot summer of 2022 in urban Chongqing. A significantly positive (negative) correlation between f(RH) and SAE ($\sigma_{sca, 525}$, or rather the pollution level) was observed on NPF days for both periods, accompanied by higher f(RH) and SAE values on NPF_{clean, HW} days. This was likely due to the observed lower FR and GR caused by possible evaporation of both unstable clusters and particle coatings under heatwaves (Bousiotis et al., 2021; Cusack et al., 2013; Deng et al., 2020; Garmash et al., 2024), thereby reducing aerosol sizes (e.g., R_{eff} , D_{mode}) while increasing SAE. Moreover, heatwave-influenced stronger photooxidation enhanced the formation

of more hygroscopic secondary components during the subsequent growth and aging processes of both pre-existing and newly formed particles on P2 NPF_{clean, HW} days in comparison to P1 NPF_{polluted} cases. The aerosol light scattering or volume concentration was mainly contributed by the larger accumulation mode particles, while more ultrafine particles dominated the size distribution, especially for the initial stage of heatwave-influenced NPF_{clean, HW} events, further leading to a lower f(RH) following NPF occurrence (i.e., $\sim 12:00-15:00$ LT) in comparison to P1 NPF_{polluted} days.

Changes in f(RH) could potentially impact the aerosol direct radiative forcing. A robust positive (negative) correlation existed between $f_{RF}(RH)$ and f(RH) (R_{eff}). Despite lower $\sigma_{sca, 525}$ during heatwaves, the corresponding mean $f_{RF}(RH)$ was relatively higher, and the maximum value of 2.21 ± 0.23 was observed on P2 NPF_{clean, HW} days, associated with the highest f(RH) (1.71 ± 0.13), smallest R_{eff} $(102.8 \pm 12.4 \,\mathrm{nm})$, and highest HBF_{525. RH} / HBF₅₂₅ ratios (1.78 ± 0.29) . The above highlights that heatwaves can influence the NPF characteristics (e.g., the evolution in the aerosol size distribution pattern and chemical composition) and atmospheric processing (although with decreased aerosol $R_{\rm eff}$ and $D_{\rm mode}$, likely due to evaporation-driven non-spherical particle morphology under persistently high temperature conditions). Further, variations in the aerosol size distribution and optical hygroscopicity under heatwaves were accompanied by elevated HBF_{525, RH} / HBF₅₂₅ ratios, potentially reducing the net solar radiation directly, especially in hot summer conditions. This study revealed divergent changes in aerosol optical and hygroscopic properties on different NPF days, thereby modulating the aerosol radiative forcing distinctly during a heatwave in the summer of 2022. A comprehensive understanding of the formation mechanisms of different NPF events (e.g., local formation versus horizontal or vertical transport) in diverse environments is crucial for the future. Last but not least, further explorations of detailed molecular-scale characterizations (e.g., molecular structures and compositions of newly and secondarily formed particles, as well as particle morphology) and aerosol radiative impacts, including aerosol-cloud interactions during heatwaves under a changing climate, are highly recommended.

Data availability. The data in this study are available at https://doi.org/10.5281/zenodo.16783914 (Hao, 2025).

Supplement. The supplement related to this article is available online at https://doi.org/10.5194/acp-25-12811-2025-supplement.

Author contributions. YH and PL: methodology, investigation, data analysis, formal analysis, visualization, validation, writing – original draft and editing. YG and ZW: methodology, investigation,

formal analysis. MT, YC, HX, and WH: data curation, methodology. FW and YL: investigation. YK: methodology, data analysis, writing – review and editing. JC: conceptualization, methodology, funding acquisition, data curation, writing – review and editing, supervision.

Competing interests. The contact author has declared that none of the authors has any competing interests.

Disclaimer. Publisher's note: Copernicus Publications remains neutral with regard to jurisdictional claims made in the text, published maps, institutional affiliations, or any other geographical representation in this paper. While Copernicus Publications makes every effort to include appropriate place names, the final responsibility lies with the authors. Views expressed in the text are those of the authors and do not necessarily reflect the views of the publisher.

Acknowledgements. This work was supported by the National Natural Science Foundation of China (grant no. 42105075) and the Venture and Innovation Support Program for Chongqing Overseas Returnees (grant no. cx2021021). We thank Biao Xue for the technical support on the utilization and maintenance of the humidified nephelometer system. We also thank Ziqian Wang for TSP filter sample collection and Jiawei Zhou for the corresponding offline chemical analysis.

Financial support. This research has been supported by the National Natural Science Foundation of China (grant no. 42105075) and the Venture and Innovation Support Program for Chongqing Overseas Returnees (grant no. cx2021021).

Review statement. This paper was edited by Imre Salma and reviewed by Junying Sun and three anonymous referees.

References

- An, J., Lu, Y., Huang, D. D., Ding, X., Hu, Q., Yan, R., Qiao, L., Zhou, M., Huang, C., Wang, H., Fu, Q., Yu, F., and Wang, L.: Sectoral Size Resolved Particle Number Emissions With Speciation: Emission Profile Based Quantification and a Case Study in the Yangtze River Delta Region, China, J. Geophys. Res.-Atmos., 1–22, https://doi.org/10.1029/2024JD041234, 2024.
- Andrews, E., Sheridan, P. J., Fiebig, M., McComiskey, A., Ogren, J. A., Arnott, P., Covert, D., Elleman, R., Gasparini, R., Collins, D., Jonsson, H., Schmid, B., and Wang, J.: Comparison of methods for deriving aerosol asymmetry parameter, J. Geophys. Res.-Atmos., 111, 1–16, https://doi.org/10.1029/2004JD005734, 2006.
- Asmi, E., Frey, A., Virkkula, A., Ehn, M., Manninen, H. E., Timonen, H., Tolonen-Kivimäki, O., Aurela, M., Hillamo, R., and Kulmala, M.: Hygroscopicity and chemical composition of Antarctic sub-micrometre aerosol particles and observations of

- new particle formation, Atmos. Chem. Phys., 10, 4253–4271, https://doi.org/10.5194/acp-10-4253-2010, 2010.
- Bae, M. S., Lee, T., Schauer, J. J., Park, G., Son, Y. B., Kim, K. H., Cho, S. S., Park, S. S., Park, K., and Shon, Z. H.: Chemical Characteristics of Size-Resolved Aerosols in Coastal Areas during KORUS-AQ Campaign; Comparison of Ion Neutralization Model, Asia-Pacific J. Atmos. Sci., 55, 387–399, https://doi.org/10.1007/s13143-018-00099-1, 2019.
- Bousiotis, D., Brean, J., Pope, F. D., Dall'Osto, M., Querol, X., Alastuey, A., Perez, N., Petäjä, T., Massling, A., Nøjgaard, J. K., Nordstrøm, C., Kouvarakis, G., Vratolis, S., Eleftheriadis, K., Niemi, J. V., Portin, H., Wiedensohler, A., Weinhold, K., Merkel, M., Tuch, T., and Harrison, R. M.: The effect of meteorological conditions and atmospheric composition in the occurrence and development of new particle formation (NPF) events in Europe, Atmos. Chem. Phys., 21, 3345–3370, https://doi.org/10.5194/acp-21-3345-2021, 2021.
- Brooke Anderson, G. and Bell, M. L.: Heat waves in the United States: Mortality risk during heat waves and effect modification by heat wave characteristics in 43 U.S. communities, Environ. Health Perspect., 119, 210–218, https://doi.org/10.1289/ehp.1002313, 2011.
- Cai, R., Chandra, I., Yang, D., Yao, L., Fu, Y., Li, X., Lu, Y., Luo, L., Hao, J., Ma, Y., Wang, L., Zheng, J., Seto, T., and Jiang, J.: Estimating the influence of transport on aerosol size distributions during new particle formation events, Atmos. Chem. Phys., 18, 16587–16599, https://doi.org/10.5194/acp-18-16587-2018, 2018.
- Chen, J., Zhao, C. S., Ma, N., and Yan, P.: Aerosol hygroscopicity parameter derived from the light scattering enhancement factor measurements in the North China Plain, Atmos. Chem. Phys., 14, 8105–8118, https://doi.org/10.5194/acp-14-8105-2014, 2014.
- Chen, Q., Mu, Z., Song, W., Wang, Y., Yang, Z., Zhang, L., and Zhang, Y. L.: Size-Resolved Characterization of the Chromophores in Atmospheric Particulate Matter From a Typical Coal-Burning City in China, J. Geophys. Res.-Atmos., 124, 10546–10563, https://doi.org/10.1029/2019JD031149, 2019.
- Chen, T., Wang, T., Xue, L., and Brasseur, G.: Heatwave exacerbates air pollution in China through intertwined climate-energy-environment interactions, Sci. Bull., 69, 2765–2775, https://doi.org/10.1016/j.scib.2024.05.018, 2024.
- China Meteorological Administration: China Climate Bulletin 2022, https://www.cma.gov.cn/zfxxgk/gknr/qxbg/202303/t20230324_5396394.html (last access: 23 March 2023), 2022 (in Chinese).
- Cheung, H. C., Chou, C. C.-K., Lee, C. S. L., Kuo, W.-C., and Chang, S.-C.: Hygroscopic properties and cloud condensation nuclei activity of atmospheric aerosols under the influences of Asian continental outflow and new particle formation at a coastal site in eastern Asia, Atmos. Chem. Phys., 20, 5911–5922, https://doi.org/10.5194/acp-20-5911-2020, 2020.
- Chylek, P. and Wong, J.: Effect of absorbing aerosols on global radiation budget, Geophys. Res. Lett., 22, 929–931, https://doi.org/10.1029/95GL00800, 1995.
- Collaud Coen, M., Weingartner, E., Nyeki, S., Cozic, J., Henning, S., Verheggen, B., Gehrig, R., and Baltensperger, U.: Long-term trend analysis of aerosol variables at the high-alpine site Jungfraujoch, J. Geophys. Res.-Atmos., 112, https://doi.org/10.1029/2006JD007995, 2007.

- Covert, D. S., Charlson, R. J., and Ahlquist, N. C.: A Study of the Relationship of Chemical Composition and Humidity to Light Scattering by Aerosols, J. Appl. Meteorol., 11, 968–976, https://doi.org/10.1175/1520-0450(1972)011<0968:asotro>2.0.co;2, 1972.
- Crumeyrolle, S., Kontkanen, J. S. S., Rose, C., Velazquez Garcia,
 A., Bourrianne, E., Catalfamo, M., Riffault, V., Tison, E., Ferreira de Brito, J., Visez, N., Ferlay, N., Auriol, F., and Chiapello,
 I.: Measurement report: Atmospheric new particle formation at a peri-urban site in Lille, northern France, Atmos. Chem. Phys.,
 23, 183–201, https://doi.org/10.5194/acp-23-183-2023, 2023.
- Cusack, M., Alastuey, A., and Querol, X.: Case studies of new particle formation and evaporation processes in the western Mediterranean regional background, Atmos. Environ., 81, 651– 659, https://doi.org/10.1016/j.atmosenv.2013.09.025, 2013.
- Dada, L., Paasonen, P., Nieminen, T., Buenrostro Mazon, S., Kontkanen, J., Peräkylä, O., Lehtipalo, K., Hussein, T., Petäjä, T., Kerminen, V.-M., Bäck, J., and Kulmala, M.: Long-term analysis of clear-sky new particle formation events and nonevents in Hyytiälä, Atmos. Chem. Phys., 17, 6227–6241, https://doi.org/10.5194/acp-17-6227-2017, 2017.
- Dal Maso, M., Kulmala, M., Riipinen, I., Wagner, R., Hussein, T., Aalto, P. P., and Lehtinen, K. E. J.: Formation and growth of fresh atmospheric aerosols: Eight years of aerosol size distribution data from SMEAR II, Hyytiälä, Finland, Boreal Environ. Res., 10, 323–336, 2005.
- Delene, D. J. and Ogren, J. A.: Variability of aerosol optical properties at four North American surface monitoring sites, J. Atmos. Sci., 59, 1135–1150, https://doi.org/10.1175/1520-0469(2002)059<1135:VOAOPA>2.0.CO;2, 2002.
- Deng, C., Fu, Y., Dada, L., Yan, C., Cai, R., Yang, D., Zhou, Y., Yin, R., Lu, Y., Li, X., Qiao, X., Fan, X., Nie, W., Kontkanen, J., Kangasluoma, J., Chu, B., Ding, A., Kerminen, V. M., Paasonen, P., Worsnop, D. R., Bianchi, F., Liu, Y., Zheng, J., Wang, L., Kulmala, M., and Jiang, J.: Seasonal characteristics of new particle formation and growth in urban Beijing, Environ. Sci. Technol., 54, 8547–8557, https://doi.org/10.1021/acs.est.0c00808, 2020.
- Deng, C., Cai, R., Yan, C., Zheng, J., and Jiang, J.: Formation and growth of sub-3 nm particles in megacities: Impact of background aerosols, Faraday Discuss., 226, 348–363, https://doi.org/10.1039/d0fd00083c, 2021.
- Duan, J., Huang, R.-J., Wang, Y., Xu, W., Zhong, H., Lin, C., Huang, W., Gu, Y., Ovadnevaite, J., Ceburnis, D., and O'Dowd, C.: Measurement report: Size-resolved secondary organic aerosol formation modulated by aerosol water uptake in wintertime haze, Atmos. Chem. Phys., 24, 7687–7698, https://doi.org/10.5194/acp-24-7687-2024, 2024.
- Fan, J., Wang, Y., Rosenfeld, D., and Liu, X.: Review of aerosolcloud interactions: Mechanisms, significance, and challenges, J. Atmos. Sci., 73, 4221–4252, https://doi.org/10.1175/JAS-D-16-0037.1, 2016.
- Fierz-Schmidhauser, R., Zieger, P., Gysel, M., Kammermann, L., DeCarlo, P. F., Baltensperger, U., and Weingartner, E.: Measured and predicted aerosol light scattering enhancement factors at the high alpine site Jungfraujoch, Atmos. Chem. Phys., 10, 2319– 2333, https://doi.org/10.5194/acp-10-2319-2010, 2010.
- Garmash, O., Ezhova, E., Arshinov, M., Belan, B., Lampilahti, A., Davydov, D., Räty, M., Aliaga, D., Baalbaki, R., Chan, T., Bianchi, F., Kerminen, V. M., Petäjä, T., and Kul-

- mala, M.: Heatwave reveals potential for enhanced aerosol formation in Siberian boreal forest, Environ. Res. Lett., 19, https://doi.org/10.1088/1748-9326/ad10d5, 2024.
- Giordano, M., Espinoza, C., and Asa-Awuku, A.: Experimentally measured morphology of biomass burning aerosol and its impacts on CCN ability, Atmos. Chem. Phys., 15, 1807–1821, https://doi.org/10.5194/acp-15-1807-2015, 2015.
- Gu, Y., Huang, R.-J., Duan, J., Xu, W., Lin, C., Zhong, H., Wang, Y., Ni, H., Liu, Q., Xu, R., Wang, L., and Li, Y. J.: Multiple pathways for the formation of secondary organic aerosol in the North China Plain in summer, Atmos. Chem. Phys., 23, 5419–5433, https://doi.org/10.5194/acp-23-5419-2023, 2023.
- Guenther, A. B., Monson, R. K., and Fall, R.: Isoprene and monoterpene emission rate variability: Observations with eucalyptus and emission rate algorithm development, J. Geophys. Res.-Atmos., 96, 10799–10808, https://doi.org/10.1029/91jd00960, 1991.
- Guo, X., Huang, J., Luo, Y., Zhao, Z., and Xu, Y.: Projection of heat waves over China for eight different global warming targets using 12 CMIP5 models, Theor. Appl. Climatol., 128, 507–522, https://doi.org/10.1007/s00704-015-1718-1, 2016.
- Hamed, A., Joutsensaari, J., Mikkonen, S., Sogacheva, L., Dal Maso, M., Kulmala, M., Cavalli, F., Fuzzi, S., Facchini, M. C., Decesari, S., Mircea, M., Lehtinen, K. E. J., and Laaksonen, A.: Nucleation and growth of new particles in Po Valley, Italy, Atmos. Chem. Phys., 7, 355–376, https://doi.org/10.5194/acp-7-355-2007, 2007.
- Hamed, A., Korhonen, H., Sihto, S. L., Joutsensaari, J., Jrvinen, H., Petäjä, T., Arnold, F., Nieminen, T., Kulmala, M., Smith, J. N., Lehtinen, K. E. J., and Laaksonen, A.: The role of relative humidity in continental new particle formation, J. Geophys. Res.-Atmos., 116, 1–12, https://doi.org/10.1029/2010JD014186, 2011
- Hand, J. L. and Malm, W. C.: Review of aerosol mass scattering efficiencies from ground-based measurements since 1990, J. Geophys. Res.-Atmos., 112, https://doi.org/10.1029/2007JD008484, 2007
- Hao, Y.: Measurements of aerosol optical hygroscopicity and aerosol size distribution under heatwaves, Zenodo [data set], https://doi.org/10.5281/zenodo.16783914, 2025.
- Hao, Y., Gou, Y., Wang, Z., Huang, W., Wan, F., Tian, M., and Chen, J.: Current challenges in the visibility improvement of urban Chongqing in Southwest China: From the perspective of PM2.5bound water uptake property over 2015–2021, Atmos. Res., 300, 107215, https://doi.org/10.1016/j.atmosres.2023.107215, 2024.
- Hao, Z., Chen, Y., Feng, S., Liao, Z., An, N., and Li, P.: The 2022 Sichuan-Chongqing spatio-temporally compound extremes: a bitter taste of novel hazards, Sci. Bull., 68, 1337–1339, https://doi.org/10.1016/j.scib.2023.05.034, 2023.
- Hauser, M., Orth, R., and Seneviratne, S. I.: Role of soil moisture versus recent climate change for the 2010 heat wave in western Russia, Geophys. Res. Lett., 43, 2819–2826, https://doi.org/10.1002/2016GL068036, 2016.
- Jefferson, A., Hageman, D., Morrow, H., Mei, F., and Watson, T.: Seven years of aerosol scattering hygroscopic growth measurements from SGP: Factors influencing water uptake, J. Geophys. Res.-Atmos., 122, 9451–9466, https://doi.org/10.1002/2017JD026804, 2017.
- Jin, X., Li, Z., Wu, T., Wang, Y., Cheng, Y., Su, T., Wei, J., Ren, R., Wu, H., Li, S., Zhang, D., and Cribb, M.: The different sensitivi-

- ties of aerosol optical properties to particle concentration, humidity, and hygroscopicity between the surface level and the upper boundary layer in Guangzhou, China, Sci. Total Environ., 803, 150010, https://doi.org/10.1016/j.scitotenv.2021.150010, 2022.
- Kerminen, V. M., Chen, X., Vakkari, V., Petäjä, T., Kulmala, M., and Bianchi, F.: Atmospheric new particle formation and growth: Review of field observations, Environ. Res. Lett., 13, https://doi.org/10.1088/1748-9326/aadf3c, 2018.
- Kim, N., Yum, S. S., Park, M., Park, J. S., Shin, H. J., and Ahn, J. Y.: Hygroscopicity of urban aerosols and its link to size-resolved chemical composition during spring and summer in Seoul, Korea, Atmos. Chem. Phys., 20, 11245–11262, https://doi.org/10.5194/acp-20-11245-2020, 2020.
- Kotchenruther, R. A., Hobbs, P. V., and Hegg, D. A.: Humidification factors for atmospheric aerosols off the mid-Atlantic coast of the United States, J. Geophys. Res.-Atmos., 104, 2239–2251, https://doi.org/10.1029/98JD01751, 1999.
- Kuang, Y., Zhao, C., Tao, J., Bian, Y., Ma, N., and Zhao, G.: A novel method for deriving the aerosol hygroscopicity parameter based only on measurements from a humidified nephelometer system, Atmos. Chem. Phys., 17, 6651–6662, https://doi.org/10.5194/acp-17-6651-2017, 2017.
- Kuang, Y., Zhao, C. S., Zhao, G., Tao, J. C., Xu, W., Ma, N., and Bian, Y. X.: A novel method for calculating ambient aerosol liquid water content based on measurements of a humidified nephelometer system, Atmos. Meas. Tech., 11, 2967–2982, https://doi.org/10.5194/amt-11-2967-2018, 2018.
- Kuang, Y., He, Y., Xu, W., Zhao, P., Cheng, Y., Zhao, G., Tao, J., Ma, N., Su, H., Zhang, Y., Sun, J., Cheng, P., Yang, W., Zhang, S., Wu, C., Sun, Y., and Zhao, C.: Distinct diurnal variation in organic aerosol hygroscopicity and its relationship with oxygenated organic aerosol, Atmos. Chem. Phys., 20, 865–880, https://doi.org/10.5194/acp-20-865-2020, 2020.
- Kulmala, M.: How Particles Nucleate and Grow, Science, 302, 1000–1001, https://doi.org/10.1126/science.1090848, 2003.
- Kulmala, M., Petäjä, T., Nieminen, T., Sipilä, M., Manninen, H. E., Lehtipalo, K., Dal Maso, M., Aalto, P. P., Junninen, H., Paasonen, P., Riipinen, I., Lehtinen, K. E. J., Laaksonen, A., and Kerminen, V. M.: Measurement of the nucleation of atmospheric aerosol particles, Nat. Protoc., 7, 1651–1667, https://doi.org/10.1038/nprot.2012.091, 2012.
- Kulmala, M., Dada, L., Daellenbach, K. R., Yan, C., Stolzenburg, D., Kontkanen, J., Ezhova, E., Hakala, S., Tuovinen, S., Kokkonen, T. V., Kurppa, M., Cai, R., Zhou, Y., Yin, R., Baalbaki, R., Chan, T., Chu, B., Deng, C., Fu, Y., Ge, M., He, H., Heikkinen, L., Junninen, H., Liu, Y., Lu, Y., Nie, W., Rusanen, A., Vakkari, V., Wang, Y., Yang, G., Yao, L., Zheng, J., Kujansuu, J., Kangasluoma, J., Petaja, T., Paasonen, P., Jarvi, L., Worsnop, D., Ding, A., Liu, Y., Wang, L., Jiang, J., Bianchi, F., and Kerminen, V. M.: Is reducing new particle formation a plausible solution to mitigate particulate air pollution in Beijing and other Chinese megacities?, Faraday Discuss., 226, 334–347, https://doi.org/10.1039/d0fd00078g, 2021.
- Kurtén, T., Torpo, L., Ding, C. G., Vehkamäki, H., Sundberg, M. R., Laasonen, K., and Kulmala, M.: A density functional study on water-sulfuric acid-ammonia clusters and implications for atmospheric cluster formation, J. Geophys. Res.-Atmos., 112, 1–7, https://doi.org/10.1029/2006JD007391, 2007.

- Lai, S., Hai, S., Gao, Y., Wang, Y., Sheng, L., Lupascu, A., Ding, A., Nie, W., Qi, X., Huang, X., Chi, X., Zhao, C., Zhao, B., Shrivastava, M., Fast, J. D., Yao, X., and Gao, H.: The striking effect of vertical mixing in the planetary boundary layer on new particle formation in the Yangtze River Delta, Sci. Total Environ., 829, 154607, https://doi.org/10.1016/j.scitotenv.2022.154607, 2022.
- Lee, K., Chandra, I., Seto, T., Inomata, Y., Hayashi, M., Takami, A., Yoshino, A., and Otani, Y.: Aerial observation of atmospheric nanoparticles on Fukue Island, Japan, Aerosol Air Qual. Res., 19, 981–994, https://doi.org/10.4209/aaqr.2018.03.0077, 2019.
- Li, Y., Ding, Y., and Li, W.: Observed trends in various aspects of compound heat waves across China from 1961 to 2015, J. Meteorol. Res., 31, 455–467, https://doi.org/10.1007/s13351-017-6150-2, 2017.
- Li, Z., Tikkanen, O. P., Buchholz, A., Hao, L., Kari, E., Yli-Juuti, T., and Virtanen, A.: Effect of Decreased Temperature on the Evaporation of α-Pinene Secondary Organic Aerosol Particles, ACS Earth Sp. Chem., 3, 2775–2785, https://doi.org/10.1021/acsearthspacechem.9b00240, 2019.
- Liu, H. J., Zhao, C. S., Nekat, B., Ma, N., Wiedensohler, A., van Pinxteren, D., Spindler, G., Müller, K., and Herrmann, H.: Aerosol hygroscopicity derived from size-segregated chemical composition and its parameterization in the North China Plain, Atmos. Chem. Phys., 14, 2525–2539, https://doi.org/10.5194/acp-14-2525-2014, 2014.
- Liu, P. F., Zhao, C. S., Göbel, T., Hallbauer, E., Nowak, A., Ran, L., Xu, W. Y., Deng, Z. Z., Ma, N., Mildenberger, K., Henning, S., Stratmann, F., and Wiedensohler, A.: Hygroscopic properties of aerosol particles at high relative humidity and their diurnal variations in the North China Plain, Atmos. Chem. Phys., 11, 3479–3494, https://doi.org/10.5194/acp-11-3479-2011, 2011.
- Lu, Y., Yan, C., Fu, Y., Chen, Y., Liu, Y., Yang, G., Wang, Y., Bianchi, F., Chu, B., Zhou, Y., Yin, R., Baalbaki, R., Garmash, O., Deng, C., Wang, W., Liu, Y., Petäjä, T., Kerminen, V.-M., Jiang, J., Kulmala, M., and Wang, L.: A proxy for atmospheric daytime gaseous sulfuric acid concentration in urban Beijing, Atmos. Chem. Phys., 19, 1971–1983, https://doi.org/10.5194/acp-19-1971-2019, 2019.
- Luoma, K., Virkkula, A., Aalto, P., Petäjä, T., and Kulmala, M.: Over a 10-year record of aerosol optical properties at SMEAR II, Atmos. Chem. Phys., 19, 11363–11382, https://doi.org/10.5194/acp-19-11363-2019, 2019.
- Ma, C. Sen, Ma, G., and Pincebourde, S.: Survive a Warming Climate: Insect Responses to Extreme High Temperatures, Annu. Rev. Entomol., 66, 163–184, https://doi.org/10.1146/annurevento-041520-074454, 2021.
- Ma, N., Zhao, C., Tao, J., Wu, Z., Kecorius, S., Wang, Z., Größ, J., Liu, H., Bian, Y., Kuang, Y., Teich, M., Spindler, G., Müller, K., van Pinxteren, D., Herrmann, H., Hu, M., and Wiedensohler, A.: Variation of CCN activity during new particle formation events in the North China Plain, Atmos. Chem. Phys., 16, 8593–8607, https://doi.org/10.5194/acp-16-8593-2016, 2016.
- Marshall, S. F., Covert, D. S., and Charlson, R. J.: Relationship between asymmetry parameter and hemispheric backscatter ratio: implications for climate forcing by aerosols, Appl. Opt., 34, 5–6, 1995.
- Merikanto, J., Spracklen, D. V., Mann, G. W., Pickering, S. J., and Carslaw, K. S.: Impact of nucleation on global CCN, Atmos.

- Chem. Phys., 9, 8601–8616, https://doi.org/10.5194/acp-9-8601-2009. 2009.
- Mishchenko, M. I.: Electromagnetic scattering by nonspherical particles: A tutorial review, J. Quant. Spectrosc. Radiat. Transf., 110, 808–832, https://doi.org/10.1016/j.jqsrt.2008.12.005, 2009.
- Moise, T., Flores, J. M., and Rudich, Y.: Optical Properties of Secondary Organic Aerosols and Their Changes by Chemical Processes, Chem. Rev., 115, 4400–4439, https://doi.org/10.1021/cr5005259, 2015.
- Nairn, J. R. and Fawcett, R. J. B.: The excess heat factor: A metric for heatwave intensity and its use in classifying heatwave severity, Int. J. Environ. Res. Public Health, 12, 227–253, https://doi.org/10.3390/ijerph120100227, 2014.
- Platis, A., Altstädter, B., Wehner, B., Wildmann, N., Lampert, A., Hermann, M., Birmili, W., and Bange, J.: An Observational Case Study on the Influence of Atmospheric Boundary-Layer Dynamics on New Particle Formation, Boundary-Layer Meteorol., 158, 67–92, https://doi.org/10.1007/s10546-015-0084-y, 2016.
- Petters, M. D. and Kreidenweis, S. M.: A single parameter representation of hygroscopic growth and cloud condensation nucleus activity, Atmos. Chem. Phys., 7, 1961–1971, https://doi.org/10.5194/acp-7-1961-2007, 2007.
- Pierce, T. E. and Waldruff, P. S.: Pc-beis: A personal computer version of the biogenic emissions inventory system, J. Air Waste Manag. Assoc., 41, 937–941, https://doi.org/10.1080/10473289.1991.10466890, 1991.
- Quinn, P. K., Bates, T. S., Baynard, T., Clarke, A. D., Onasch, T. B., Wang, W., Rood, M. J., Andrews, E., Allan, J., Carrico, C. M., Coffman, D., and Worsnop, D.: Impact of particulate organic matter on the relative humidity dependence of light scattering: A simplified parameterization, Geophys. Res. Lett., 32, 1–4, https://doi.org/10.1029/2005GL024322, 2005.
- Ren, J., Chen, L., Fan, T., Liu, J., Jiang, S., and Zhang, F.: The NPF Effect on CCN Number Concentrations: A Review and Re-Evaluation of Observations From 35 Sites Worldwide, Geophys. Res. Lett., 48, 1–12, https://doi.org/10.1029/2021GL095190, 2021.
- Rosati, B., Isokääntä, S., Christiansen, S., Jensen, M. M., Moosakutty, S. P., Wollesen de Jonge, R., Massling, A., Glasius, M., Elm, J., Virtanen, A., and Bilde, M.: Hygroscopicity and CCN potential of DMS-derived aerosol particles, Atmos. Chem. Phys., 22, 13449–13466, https://doi.org/10.5194/acp-22-13449-2022, 2022.
- Salma, I., Németh, Z., Kerminen, V. M., Aalto, P., Nieminen, T., Weidinger, T., Molnár, Á., Imre, K., and Kulmala, M.: Regional effect on urban atmospheric nucleation, Atmos. Chem. Phys., 16, 8715–8728, https://doi.org/10.5194/acp-16-8715-2016, 2016.
- Schuster, G. L., Dubovik, O., and Holben, B. N.: Angstrom exponent and bimodal aerosol size distributions, J. Geophys. Res.-Atmos., 111, 1–14, https://doi.org/10.1029/2005JD006328, 2006.
- Shang, D., Hu, M., Tang, L., Fang, X., Liu, Y., Wu, Y., Du, Z., Cai, X., Wu, Z., Lou, S., Hallquist, M., Guo, S., and Zhang, Y.: Significant effects of transport on nanoparticles during new particle formation events in the atmosphere of Beijing, Particuology, 80, 1–10, https://doi.org/10.1016/j.partic.2022.12.006, 2023.
- Sharma, S. and Mujumdar, P.: Increasing frequency and spatial extent of concurrent meteorological droughts and heatwaves

- in India, Sci. Rep., 7, 1–9, https://doi.org/10.1038/s41598-017-15896-3, 2017.
- Shen, X. J., Sun, J. Y., Zhang, Y. M., Wehner, B., Nowak, A., Tuch, T., Zhang, X. C., Wang, T. T., Zhou, H. G., Zhang, X. L., Dong, F., Birmili, W., and Wiedensohler, A.: First long-term study of particle number size distributions and new particle formation events of regional aerosol in the North China Plain, Atmos. Chem. Phys., 11, 1565–1580, https://doi.org/10.5194/acp-11-1565-2011, 2011.
- Su, Y. W.: The effects of extreme high temperature day off on electricity conservation, Weather. Clim. Soc., 13, 769–782, https://doi.org/10.1175/WCAS-D-20-0176.1, 2021.
- Sun, J., Hermann, M., Weinhold, K., Merkel, M., Birmili, W., Yang, Y., Tuch, T., Flentje, H., Briel, B., Ries, L., Couret, C., Elsasser, M., Sohmer, R., Wirtz, K., Meinhardt, F., Schütze, M., Bath, O., Hellack, B., Kerminen, V.-M., Kulmala, M., Ma, N., and Wiedensohler, A.: Measurement report: Contribution of atmospheric new particle formation to ultrafine particle concentration, cloud condensation nuclei, and radiative forcing results from 5-year observations in central Europe, Atmos. Chem. Phys., 24, 10667–10687, https://doi.org/10.5194/acp-24-10667-2024, 2024.
- Sun, X., Sun, Q., Zhou, X., Li, X., Yang, M., Yu, A., and Geng, F.: Heat wave impact on mortality in Pudong New Area, China in 2013, Sci. Total Environ., 493, 789–794, https://doi.org/10.1016/j.scitotenv.2014.06.042, 2014.
- Sun, Y., Song, L., Yin, H., Zhang, X., Stott, P., Zhou, B., and Hu, T.: 20. Human influence on the 2015 extreme high temperature events in Western China, Bull. Am. Meteorol. Soc., 97, S102–S106, https://doi.org/10.1175/BAMS-D-16-0158.1, 2016.
- Tan, J., Zheng, Y., Song, G., Kalkstein, L. S., Kalkstein, A. J., and Tang, X.: Heat wave impacts on mortality in Shanghai, 1998 and 2003, Int. J. Biometeorol., 51, 193–200, https://doi.org/10.1007/s00484-006-0058-3, 2007.
- Tan, W., Yu, Y., Li, C., Li, J., Kang, L., Dong, H., Zeng, L., and Zhu, T.: Profiling Aerosol Liquid Water Content Using a Polarization Lidar, Environ. Sci. Technol., 54, 3129–3137, https://doi.org/10.1021/acs.est.9b07502, 2020.
- Tang, M., Chan, C. K., Li, Y. J., Su, H., Ma, Q., Wu, Z., Zhang, G., Wang, Z., Ge, M., Hu, M., He, H., and Wang, X.: A review of experimental techniques for aerosol hygroscopicity studies, Atmos. Chem. Phys., 19, 12631–12686, https://doi.org/10.5194/acp-19-12631-2019, 2019.
- Tao, L., Zhou, Z., Tao, J., Zhang, L., Wu, C., Li, J., Yue, D., Wu, Z., Zhang, Z., Yuan, Z., Huang, J., and Wang, B.: High contribution of new particle formation to ultrafine particles in four seasons in an urban atmosphere in south China, Sci. Total Environ., 889, https://doi.org/10.1016/j.scitotenv.2023.164202, 2023.
- Teng, M., Liao, H., Burke, P. J., Chen, T., and Zhang, C.: Adaptive responses: the effects of temperature levels on residential electricity use in China, Clim. Change, 172, https://doi.org/10.1007/s10584-022-03374-3, 2022.
- Tian, J., Wang, Q., Zhang, Y., Yan, M., Liu, H., Zhang, N., Ran, W., and Cao, J.: Impacts of primary emissions and secondary aerosol formation on air pollution in an urban area of China during the COVID-19 lockdown, Environ. Int., 150, 106426, https://doi.org/10.1016/j.envint.2021.106426, 2021.
- Titos, G., Jefferson, A., Sheridan, P. J., Andrews, E., Lyamani, H., Alados-Arboledas, L., and Ogren, J. A.: Aerosol

- light-scattering enhancement due to water uptake during the TCAP campaign, Atmos. Chem. Phys., 14, 7031–7043, https://doi.org/10.5194/acp-14-7031-2014, 2014.
- Titos, G., Cazorla, A., Zieger, P., Andrews, E., Lyamani, H., Granados-Muñoz, M. J., Olmo, F. J., and Alados-Arboledas, L.: Effect of hygroscopic growth on the aerosol light-scattering coefficient: A review of measurements, techniques and error sources, Atmos. Environ., 141, 494–507, https://doi.org/10.1016/j.atmosenv.2016.07.021, 2016.
- Titos, G., Burgos, M. A., Zieger, P., Alados-Arboledas, L., Baltensperger, U., Jefferson, A., Sherman, J., Weingartner, E., Henzing, B., Luoma, K., O'Dowd, C., Wiedensohler, A., and Andrews, E.: A global study of hygroscopicity-driven light-scattering enhancement in the context of other in situ aerosol optical properties, Atmos. Chem. Phys., 21, 13031–13050, https://doi.org/10.5194/acp-21-13031-2021, 2021.
- Tritscher, T., Jurnyi, Z., Martin, M., Chirico, R., Gysel, M., Heringa, M. F., Decarlo, P. F., Sierau, B., Prévt, A. S. H., Weingartner, E., and Baltensperger, U.: Changes of hygroscopicity and morphology during ageing of diesel soot, Environ. Res. Lett., 6, https://doi.org/10.1088/1748-9326/6/3/034026, 2011.
- Wang, N., Du, Y., Chen, D., Meng, H., Chen, X., Zhou, L., Shi, G., Zhan, Y., Feng, M., Li, W., Chen, M., Li, Z., and Yang, F.: Spatial disparities of ozone pollution in the Sichuan Basin spurred by extreme, hot weather, Atmos. Chem. Phys., 24, 3029–3042, https://doi.org/10.5194/acp-24-3029-2024, 2024.
- Wang, Y., Li, Z., Zhang, R., Jin, X., Xu, W., Fan, X., Wu, H., Zhang, F., Sun, Y., Wang, Q., Cribb, M., and Hu, D.: Distinct Ultrafine-and Accumulation-Mode Particle Properties in Clean and Polluted Urban Environments, Geophys. Res. Lett., 46, 10918–10925, https://doi.org/10.1029/2019GL084047, 2019.
- Wang, Z. B., Hu, M., Sun, J. Y., Wu, Z. J., Yue, D. L., Shen, X. J., Zhang, Y. M., Pei, X. Y., Cheng, Y. F., and Wiedensohler, A.: Characteristics of regional new particle formation in urban and regional background environments in the North China Plain, Atmos. Chem. Phys., 13, 12495–12506, https://doi.org/10.5194/acp-13-12495-2013, 2013.
- Wang, Z., Wu, Z., Yue, D., Shang, D., Guo, S., Sun, J., Ding, A., Wang, L., Jiang, J., Guo, H., Gao, J., Cheung, H. C., Morawska, L., Keywood, M., and Hu, M.: New particle formation in China: Current knowledge and further directions, Sci. Total Environ., 577, 258–266, https://doi.org/10.1016/j.scitotenv.2016.10.177, 2017.
- Westervelt, D. M., Pierce, J. R., Riipinen, I., Trivitayanurak, W., Hamed, A., Kulmala, M., Laaksonen, A., Decesari, S., and Adams, P. J.: Formation and growth of nucleated particles into cloud condensation nuclei: model–measurement comparison, Atmos. Chem. Phys., 13, 7645–7663, https://doi.org/10.5194/acp-13-7645-2013, 2013.
- Wu, Z. J., Poulain, L., Birmili, W., Größ, J., Niedermeier, N., Wang, Z. B., Herrmann, H., and Wiedensohler, A.: Some insights into the condensing vapors driving new particle growth to CCN sizes on the basis of hygroscopicity measurements, Atmos. Chem. Phys., 15, 13071–13083, https://doi.org/10.5194/acp-15-13071-2015, 2015.
- Wu, Z. J., Zheng, J., Shang, D. J., Du, Z. F., Wu, Y. S., Zeng, L.M., Wiedensohler, A., and Hu, M.: Particle hygroscopicity and its link to chemical composition in the urban atmosphere of Bei-

- jing, China, during summertime, Atmos. Chem. Phys., 16, 1123–1138, https://doi.org/10.5194/acp-16-1123-2016, 2016.
- Xia, C., Sun, J., Hu, X., Shen, X., Zhang, Y., Zhang, S., Wang, J., Liu, Q., Lu, J., Liu, S., and Zhang, X.: Effects of hygroscopicity on aerosol optical properties and direct radiative forcing in Beijing: Based on two-year observations, Sci. Total Environ., 857, 159233, https://doi.org/10.1016/j.scitotenv.2022.159233, 2023.
- Xu, W., Chen, C., Qiu, Y., Xie, C., Chen, Y., Ma, N., Xu, W., Fu, P., Wang, Z., Pan, X., Zhu, J., Ngcg, N. L., and Sun, Y.: Size-resolved characterization of organic aerosol in the North China Plain: New insights from high resolution spectral analysis, Environ. Sci. Atmos., 1, 346–358, https://doi.org/10.1039/d1ea00025j, 2021.
- Xu, W., Kuang, Y., Xu, W., Zhang, Z., Luo, B., Zhang, X., Tao, J., Qiao, H., Liu, L., and Sun, Y.: Hygroscopic growth and activation changed submicron aerosol composition and properties in the North China Plain, Atmos. Chem. Phys., 24, 9387–9399, https://doi.org/10.5194/acp-24-9387-2024, 2024.
- Xu, W. Y., Zhao, C. S., Ran, L., Deng, Z. Z., Liu, P. F., Ma, N., Lin, W. L., Xu, X. B., Yan, P., He, X., Yu, J., Liang, W. D., and Chen, L. L.: Characteristics of pollutants and their correlation to meteorological conditions at a suburban site in the North China Plain, Atmos. Chem. Phys., 11, 4353–4369, https://doi.org/10.5194/acp-11-4353-2011, 2011.
- Xue, B., Kuang, Y., Xu, W., and Zhao, P.: Joint increase of aerosol scattering efficiency and aerosol hygroscopicity aggravate visibility impairment in the North China Plain, Sci. Total Environ., 839, 141163, https://doi.org/10.1016/j.scitotenv.2022.156279, 2022.
- Yang, P., Feng, Q., Hong, G., Kattawar, G. W., Wiscombe, W. J., Mishchenko, M. I., Dubovik, O., Laszlo, I., and Sokolik, I. N.: Modeling of the scattering and radiative properties of nonspherical dust-like aerosols, J. Aerosol Sci., 38, 995–1014, https://doi.org/10.1016/j.jaerosci.2007.07.001, 2007.
- Yarragunta, Y., Srivastava, S., Mitra, D., and Chandola, H. C.: Source apportionment of carbon monoxide over India: a quantitative analysis using MOZART-4, Environ. Sci. Pollut. Res., 28, 8722–8742, https://doi.org/10.1007/s11356-020-11099-y, 2021.
- Yuan, L. and Zhao, C.: Quantifying particle-to-particle heterogeneity in aerosol hygroscopicity, Atmos. Chem. Phys., 23, 3195–3205, https://doi.org/10.5194/acp-23-3195-2023, 2023.
- Zhang, L., Sun, J. Y., Shen, X. J., Zhang, Y. M., Che, H., Ma, Q. L., Zhang, Y. W., Zhang, X. Y., and Ogren, J. A.: Observations of relative humidity effects on aerosol light scattering in the Yangtze River Delta of China, Atmos. Chem. Phys., 15, 8439–8454, https://doi.org/10.5194/acp-15-8439-2015, 2015.
- Zhang, R., Suh, I., Zhao, J., Zhang, D., Fortner, E. C., Tie, X., Molina, L. T., and Molina, M. J.: Atmospheric new particle formation enhanced by organic acids, Science, 304, 1487–1490, https://doi.org/10.1126/science.1095139, 2004.
- Zhang, R., Khalizov, A. F., Pagels, J., Zhang, D., Xue, H., and McMurry, P. H.: Variability in morphology, hygroscopicity, and optical properties of soot aerosols during atmospheric processing, Proc. Natl. Acad. Sci. U. S. A., 105, 10291–10296, https://doi.org/10.1073/pnas.0804860105, 2008.
- Zhang, R., Khalizov, A., Wang, L., Hu, M., and Xu, W.: Nucleation and growth of nanoparticles in the atmosphere, Chem. Rev., 112, 1957–2011, https://doi.org/10.1021/cr2001756, 2012.

- Zhang, R., Wang, G., Guo, S., Zamora, M. L., Ying, Q., Lin, Y., Wang, W., Hu, M., and Wang, Y.: Formation of Urban Fine Particulate Matter, Chem. Rev., 115, 3803–3855, https://doi.org/10.1021/acs.chemrev.5b00067, 2015.
- Zhang, Z., Xu, W., Zeng, S., Liu, Y., Liu, T., Zhang, Y., Du, A., Li, Y., Zhang, N., Wang, J., Aruffo, E., Han, P., Li, J., Wang, Z., and Sun, Y.: Secondary Organic Aerosol Formation from Ambient Air in Summer in Urban Beijing: Contribution of S/IVOCs and Impacts of Heat Waves, Environ. Sci. Technol. Lett., https://doi.org/10.1021/acs.estlett.4c00415, 2024.
- Zhao, C., Yu, Y., Kuang, Y., Tao, J., and Zhao, G.: Recent Progress of Aerosol Light-scattering Enhancement Factor Studies in China, Adv. Atmos. Sci., 36, 1015–1026, https://doi.org/10.1007/s00376-019-8248-1, 2019.
- Zhao, G., Hu, M., Fang, X., Tan, T., Xiao, Y., Du, Z., Zheng, J., Shang, D., Wu, Z., Guo, S., and Zhao, C.: Larger than expected variation range in the real part of the refractive index for ambient aerosols in China, Sci. Total Environ., 779, 146443, https://doi.org/10.1016/j.scitotenv.2021.146443, 2021.
- Zhao, S., Yu, Y., Li, J., Yin, D., Qi, S., and Qin, D.: Response of particle number concentrations to the clean air action plan: lessons from the first long-term aerosol measurements in a typical urban valley in western China, Atmos. Chem. Phys., 21, 14959–14981, https://doi.org/10.5194/acp-21-14959-2021, 2021.

- Zhu, Y., Shen, Y., Li, K., Meng, H., Sun, Y., Yao, X., Gao, H., Xue, L., and Wang, W.: Investigation of Particle Number Concentrations and New Particle Formation With Largely Reduced Air Pollutant Emissions at a Coastal Semi-Urban Site in Northern China, J. Geophys. Res.-Atmos., 126, 1–20, https://doi.org/10.1029/2021JD035419, 2021.
- Zieger, P., Weingartner, E., Henzing, J., Moerman, M., de Leeuw, G., Mikkilä, J., Ehn, M., Petäjä, T., Clémer, K., van Roozendael, M., Yilmaz, S., Frieß, U., Irie, H., Wagner, T., Shaiganfar, R., Beirle, S., Apituley, A., Wilson, K., and Baltensperger, U.: Comparison of ambient aerosol extinction coefficients obtained from in-situ, MAX-DOAS and LIDAR measurements at Cabauw, Atmos. Chem. Phys., 11, 2603–2624, https://doi.org/10.5194/acp-11-2603-2011, 2011.